Transportation Research Part B 94 (2016) 314–334

Contents lists available at ScienceDirect

Transportation Research Part B

journal homepage: www.elsevier.com/locate/trb

Constrained optimization and distributed computation based car following control of a connected and autonomous vehicle platoon

Siyuan Gong[a], Jinglai Shen[b], Lili Du[a,*]

[a] Department of Civil, Architectural and Environmental Engineering, Illinois Institute of Technology, Chicago, IL 60616, USA
[b] Department of Mathematics and Statistics, University of Maryland Baltimore County, MD 21250, USA

ARTICLE INFO

Article history:
Received 18 June 2016
Revised 29 September 2016
Accepted 30 September 2016
Available online 14 October 2016

Keywords:
Connected and autonomous vehicles
Car-following control
Optimization
Distributed algorithm

ABSTRACT

Motivated by the advancement in connected and autonomous vehicle technologies, this paper develops a novel car-following control scheme for a platoon of connected and autonomous vehicles on a straight highway. The platoon is modeled as an interconnected multi-agent dynamical system subject to physical and safety constraints, and it uses the global information structure such that each vehicle shares information with all the other vehicles. A constrained optimization based control scheme is proposed to ensure an entire platoon's transient traffic smoothness and asymptotic dynamic performance. By exploiting the solution properties of the underlying optimization problem and using primal-dual formulation, this paper develops dual based distributed algorithms to compute optimal solutions with proven convergence. Furthermore, the asymptotic stability of the unconstrained linear closed-loop system is established. These stability analysis results provide a principle to select penalty weights in the underlying optimization problem to achieve the desired closed-loop performance for both the transient and the asymptotic dynamics. Extensive numerical simulations are conducted to validate the efficiency of the proposed algorithms.

1. Introduction

For traditional human-driven vehicles, drivers determine car-following behaviors, i.e., acceleration or deceleration, speed, and spacing between adjacent vehicles, according to drivers' own sensitivity and reaction time to their leading vehicles' movement variations (May, 1989). Experimental and theoretical results have shown that improper car-following behaviors, e.g., overreacting or timid car-following, are one of the key factors to trigger traffic congestion, oscillations (stop-and-go or slow-and-fast traffic), and accidents (Laval and Leclercq, 2010). However, due to high randomness and inhomogeneity of human drivers' behaviors, few technologies can be implemented to control car-following behaviors of human-driven vehicles and to improve traffic performance. As a result, the current traffic flows often demonstrate low efficiency and have severe environmental impact in many urban areas.

The recent advancement of connected and autonomous vehicle technologies provides tremendous opportunities for developing coordinated car-following control of multiple vehicles that promote driving safety and efficiency and mitigate

* Corresponding author.
E-mail addresses: sgong1@hawk.iit.edu (S. Gong), shenj@umbc.edu (J. Shen), ldu3@iit.edu (L. Du).

http://dx.doi.org/10.1016/j.trb.2016.09.016
0191-2615/

negative environmental impact. In particular, connected vehicle technologies, including vehicle-to-vehicle (V2V), vehicle-to-infrastructure (V2I), and vehicle-to-other-digital-facilities (V2X), enable individual vehicles to access online traffic information, accurately view nearby traffic conditions, and further communicate with other vehicles to establish coordinated or cooperative driving. In addition, autonomous vehicle technologies allow modern computation and control techniques to be implemented for advanced vehicle control to achieve neighborhood mobility and safety of individual vehicles as well as desired system performance. Hence, the goal of the present paper is to develop car-following control schemes for a platoon of vehicles by leveraging connected and autonomous technologies to enhance mobility and safety of both individual vehicles and platoon performance, e.g., reduced traffic oscillations and smoother traffic flows, which will potentially improve environmental sustainability significantly.

In the field of transportation engineering, the research of this paper is closely related to the cooperative adaptive cruise control (CACC) technologies. These technologies allow a vehicle to automatically adjust its speed to maintain a safety distance from its preceding vehicle, based on information gathered from stationary or mobile devices, but without platoon performance guarantee. The CACC technologies have been extensively studied in transportation engineering using microscopic traffic flow theory and safety policies under different information structures (Li et al., 2015), e.g., the immediate preceding structure (van Arem et al., 2006; Desjardins and Chaib-draa, 2011; Rajamani and Shladover, 2001; Shladover et al., 2001), the multiple preceding structure (van Arem et al., 2007; Swaroop and Hedrick, 1999; Schakel et al., 2010), and the preceding-and-following structure (Nakayama et al., 2002; Wang et al., 2014; Zheng et al., 2016a). These papers show improved neighborhood driving safety, traffic flow stability and efficiency. The platoon performance of the CACC technologies, e.g., traffic oscillations, also receives considerable interest in the literature. However, such the performance is mainly evaluated by simulations as extra benefits rather than being treated as a direct control objective in CACC algorithm design. Thus this line of research lacks a theoretical foundation and formal justification of effectiveness under general traffic conditions.

Car-following control for connected and autonomous vehicles has also garnered substantial attention in control engineering. From the control systems point of view, a platoon of connected and autonomous vehicles is an interconnected system, and car-following can be treated as a cooperative control problem. Various interconnecting stability issues, e.g., string stability (Swaroop, 1997; Swaroop and Hedrick, 1996), have been studied using frequency-domain methods, linear feedback theory, and Lyapunov theory, and applied to a vehicle platoon (Cook, 2007; Monteil et al., 2014; Naus et al., 2010a,b; Oncu et al., 2014). Linear robust control theory is exploited for performance analysis under different data exchange structures (Hao and Barooah, 2013; Jovanović and Bamieh, 2005; Lin et al., 2012; Middleton and Braslavsky, 2010). Communication delays and other disturbances are also considered (Jin and Orosz, 2014; Qin et al., 2014; Seiler et al., 2004). Most research along this line focuses on asymptotic dynamics and stability; transient traffic dynamics, e.g., traffic oscillations, are not fully addressed.

An ideal car-following control scheme is expected to regulate individual vehicles' car-following behaviors and achieve desired platoon performance. Despite the extensive studies in transportation and control engineering, there remain several unsolved challenges to establish such car-following control. We discuss three major challenges that motivate the research of this paper as follows. (i) Multiple objective are often introduced by desired platoon performance. A vehicle platoon is a complex engineering system, and control design is expected to meet multiple, possibly conflicting, objectives in terms of transient and asymptotic dynamics, including mobility, safety, and traffic dynamic stability. But the transient dynamics issues receive much less attention in the control literature. Furthermore, the conventional CACC technologies mainly focus on individual vehicle's mobility and safety requirements, which may be conflicting to platoon performance. (ii) Achieving desired platoon performance needs to take traffic constraints into account, since connected and autonomous vehicles are subject to various inequality constraints due to physical limitations, safety concerns, and driving comfort consideration. This yields state and control coupled constraints that turn a platoon into a constrained dynamical system and give rise to many difficulties in control design. While certain constraints have been addressed in Cook (2007); Dunbar and Murray (2006); Keviczky et al. (2006); Richards and How (2004), these results often impose restrictive assumptions that are unrealistic to a platoon. (iii) To implement such platoon control, distributed computation is needed. A platoon consists of a large number of vehicles with varying topology. Due to a high computation load and the absence of roadside computing facilities, centralized computation is either inefficient or infeasible. This calls for distributed computation, which takes full advantage of an individual vehicle's computing capability and is more flexible. However, the development of distributed algorithms is rather nontrivial, especially for a system with coupled constraints. Although distributed control schemes are recently proposed in Dunbar and Caveney (2012); Dunbar and Murray (2006); Franco et al. (2008), these schemes focus on stability only, and do not handle state and control coupled constraints.

Inspired by the above-mentioned challenges, this paper develops a novel car-following control scheme based on constrained optimization and distributed computation by exploiting transportation, control and optimization techniques. This control scheme takes vehicle constraints, transient dynamics, and asymptotic dynamics into account, and can be implemented by state-of-art distributed algorithms. We summarize the major contributions of the paper as follows. Throughout the rest of the paper, all vehicles are referred to as connected and autonomous vehicles.

(1) We consider a platoon of connected and autonomous vehicles on a straight roadway, and model the platoon as a multi-agent interconnected dynamic system subject to acceleration, speed, and safety distance constraints. The platoon uses the global information structure such that each vehicle has communication and shares traffic information with all the other vehicles. To handle multiple objectives arising from transient and asymptotic dynamics under the

constraints, we introduce a constrained optimization problem whose solution determines car-following control. This optimization problem explicitly incorporates transient traffic performance into its objective function. Important properties of the optimization problem are studied; these properties build a rigorous foundation for distribute algorithm development.

(2) The underlying optimization problem is a convex quadratically constrained quadratic program, where the safety distance constraint yields a state and control coupled nonlinear constraint that poses many difficulties in developing distributed algorithms. To overcome these difficulties, we employ recent distributed algorithms for multiuser optimization in Koshal et al. (2009, 2011). Using the properties of the underlying optimization problem, the convergence of distributed algorithms is established. Extensive simulations illustrate effectiveness of the proposed algorithms.

(3) The performance of the proposed car-following control scheme is studied using systems and control theory. In particular, we focus on the constraint free scenario where the closed-loop system becomes a linear system. It is shown via stability analysis techniques that the linear closed-loop system is asymptotically stable. Moreover, the stability analysis results give a clue to choose penalty weights in the underlying optimization problem to achieve the desired closed-loop performance, for both the transient and the asymptotic dynamics.

Overall, this paper presents an advancement in addressing an important transportation problem by well integrated and rigorous optimization, control and traffic flow techniques. It will contribute to connected and autonomous vehicle technologies in both intellectual merit and practical applications.

The rest of the paper is organized as follows. The dynamic model of a platoon and its state and control constraints are introduced in Section 2. To determine car-following control, a constrained optimization problem is proposed and its important properties are studied in Section 3. By using these properties, dual based distributed algorithms are developed in Section 4. Section 5 studies the performance of the proposed control scheme, especially the linear dynamics of the closed-loop system, and determines penalty weights for desired performance. Numerical results are presented in Section 6 with concluding remarks given in Section 7.

2. Vehicle dynamics, constraints, and control objectives

Consider a platoon of multiple vehicles on a straight roadway, where the (uncontrolled) leading vehicle is labeled by the index 0 and its n following automated vehicles are labeled by the indices $i = 1, \ldots, n$ respectively. Let x_i, v_i, u_i denote the longitudinal position, speed, and acceleration of the ith vehicle respectively, where $u_i, i = 1, \ldots, n$ are control inputs. Let $\tau > 0$ be the sampling time, and the control u_i is constant on each time interval $[k\tau, (k+1)\tau)$ for $k \in \mathbb{Z}_+ := \{0, 1, 2, \ldots\}$. The discrete-time longitudinal dynamics is described by the following double-integrator model:

$$x_i(k+1) = x_i(k) + \tau v_i(k) + \frac{\tau^2}{2} u_i(k), \quad v_i(k+1) = v_i(k) + \tau u_i(k), \qquad i = 1, \ldots, n. \tag{1}$$

Here $x_i(k), v_i(k), u_i(k)$ represent $x_i(k\tau), v_i(k\tau), u_i(k\tau)$ respectively for notational simplicity. The double-integrator model (1) is widely used for system-level car following control design (Cook, 2007; Hao and Barooah, 2013; Lin et al., 2012); see Zheng et al. (2016a,b) for more complex models which include the torque dynamics and inertia effects.

The vehicles in a platoon are subject to several important state and control constraints summarized as follows. Let $i = 1, \ldots, n$.

(1) Control constraints: $a_{\min} \le u_i \le a_{\max}$, where $a_{\min} < 0$ and $a_{\max} > 0$ are pre-specified acceleration/deceleration bounds for each vehicle;

(2) Speed constraints: $v_{\min} \le v_i \le v_{\max}$, where $0 \le v_{\min} < v_{\max}$ are pre-specified bounds on longitudinal speed for each vehicle;

(3) Safety distance constraints: $x_{i-1} - x_i \ge L + r \cdot v_i - \frac{(v_i - v_{\min})^2}{2a_{\min}}$. This inequality follows from kinematic analysis, where $r \ge \tau$ is the constant reaction time due to dynamic and other delay, and $L > 0$ is a constant depending on vehicle length.

Moreover, we assume that the leading vehicle satisfies $a_{\min} \le u_0(k) \le a_{\max}$ and $v_{\min} \le v_0(k) \le v_{\max}$ for each $k \in \mathbb{Z}_+$. These inequality constraints are crucial to car-following control development.

The objectives of a car-following control scheme are two folds: (i) transient dynamics: maintain a desired safe spacing between two consecutive vehicles in a platoon, and reduce traffic flow oscillations in terms of spacing and speed changes; and (ii) asymptotic dynamics: the relative distance of two consecutive vehicles should be asymptotically stable and converge to a desired (constant) spacing. Besides it is expected that a control scheme is computed in a decentralized and distributed manner. To reach these goals, a constrained optimization approach is introduced in the next section.

3. Constrained optimization based car-following control

We propose a constrained optimization problem whose optimal solution at each time $k \in \mathbb{Z}_+$ determines the car-following control. This optimization problem takes transient dynamics of the platoon into account, and its important properties are studied in this section.

Suppose $x_0(k), v_0(k), u_0(k)$ of the leading vehicle are known at each k. Let $\Delta > L$ be the desired constant distance between two adjacent vehicles, where Δ is chosen from an interval whose lower and upper bounds are determined by

a speed limit, the reaction time r, and traffic density. Define the vectors $z(k) := (x_0 - x_1 - \Delta, \ldots, x_{n-1} - x_n - \Delta)^T(k) \in \mathbb{R}^n$, $z'(k) := (v_0 - v_1, \ldots, v_{n-1} - v_n)^T(k) \in \mathbb{R}^n$, and the control $u(k) := (u_1, \ldots, u_n)^T(k) \in \mathbb{R}^n$. It follows from (1) that at each time $k \in \mathbb{Z}_+$, the dynamics of the ith vehicle are given by

$$\begin{bmatrix} z_i(k+1) \\ z_i'(k+1) \end{bmatrix} = \begin{bmatrix} 1 & \tau \\ 0 & 1 \end{bmatrix} \begin{bmatrix} z_i(k) \\ z_i'(k) \end{bmatrix} + \begin{bmatrix} \frac{\tau^2}{2} \\ \tau \end{bmatrix} w_i(k), \qquad \forall\, i = 1, \ldots, n,$$

where $w_i(k) := u_{i-1}(k) - u_i(k)$ for each $i = 1, \ldots, n$. Letting $w(k) := (w_1(k), \ldots, w_n(k))^T \in \mathbb{R}^n$, we obtain the linear control system:

$$\begin{bmatrix} z(k+1) \\ z'(k+1) \end{bmatrix} = \begin{bmatrix} I_n & \tau I_n \\ 0 & I_n \end{bmatrix} \begin{bmatrix} z(k) \\ z'(k) \end{bmatrix} + \begin{bmatrix} \frac{\tau^2}{2} I_n \\ \tau I_n \end{bmatrix} w(k). \tag{2}$$

Let $\mathbf{1} := (1, \ldots, 1)^T \in \mathbb{R}^n$ be the vector of ones. It is easy to verify that

$$u(k) = -Sw(k) + u_0(k) \cdot \mathbf{1}, \qquad \text{where} \quad S := \begin{bmatrix} 1 & 0 & 0 & \ldots & 0 \\ 1 & 1 & 0 & \ldots & 0 \\ \vdots & \vdots & \ddots & \ddots & \vdots \\ 1 & 1 & \ldots & 1 & 0 \\ 1 & 1 & \ldots & 1 & 1 \end{bmatrix} \in \mathbb{R}^{n \times n}. \tag{3}$$

Note that S is invertible so that S^TS is positive definite. Hence $S^TS = P^T \Lambda P$ for an orthogonal matrix P and a diagonal matrix $\Lambda = \mathrm{diag}(s_1, \ldots, s_n)$ with $s_1 \geq s_2 \geq \cdots \geq s_n > 0$, where the orthogonal matrix P characterizes the control interaction of the interconnected vehicle dynamics.

Let $\alpha := (\alpha_1, \ldots, \alpha_n)$ and $\beta := (\beta_1, \ldots, \beta_n)$, where $\alpha_i > 0$ and $\beta_i > 0$ are penalty weights for each $i = 1, \ldots, n$, and two diagonal matrices $D_\alpha := \mathrm{diag}(\alpha_1, \ldots, \alpha_n)$ and $D_\beta := \mathrm{diag}(\beta_1, \ldots, \beta_n)$. Further, let $Q_z := P^T D_\alpha P$ and $Q_{z'} := P^T D_\beta P$ be symmetric and positive definite matrices, and $\| \cdot \|_2$ be the Euclidean norm. Define the objective function of quadratic form

$$J(u(k)) := \frac{1}{2} z^T(k+1) Q_z z(k+1) + \frac{1}{2} (z'(k+1))^T Q_{z'} z'(k+1) + \frac{\tau^2}{2} \|u(k)\|_2^2. \tag{4}$$

Here the three terms in J intend to minimize traffic flow oscillations using mild control at time $k+1$, under suitable penalty weights α and β. Particularly, the first term pertains to the penalty on the relative spacing variation, the second term pertains to the penalty on the relative speed variation, and the last term characterizes the magnitude of control. The weight matrices Q_z and $Q_{z'}$ are chosen in the above form such that the penalty weights α_i's and β_i's directly affect the closed-loop dynamics (cf. Section 5). This choice not only facilitates close-loop dynamics analysis but also takes the control interactions of the interconnected vehicle dynamics into account, which leads to better closed-loop performance. Specific choices of α and β to achieve the desired transient and asymptotic dynamics will be discussed in Section 5. At each $k \in \mathbb{Z}_+$, the control $u(k)$ is determined by the following constrained optimization problem for the given $(x_i(k), v_i(k))_{i=0}^n$ and $u_0(k)$:

$$\text{minimize} \quad J(u(k)) \tag{5}$$

subject to: for each $i = 1, \ldots, n$,

$$a_{\min} \leq u_i(k) \leq a_{\max}, \tag{6}$$

$$v_{\min} \leq v_i(k+1) \leq v_{\max}, \tag{7}$$

$$x_{i-1}(k+1) - x_i(k+1) \geq L + r \cdot v_i(k+1) - \frac{(v_i(k+1) - v_{\min})^2}{2a_{\min}}, \tag{8}$$

where $r \geq \tau$, and $v_i(k+1), x_i(k+1)$ are given in term of $u(k)$ in (1), that is, $x_i(k+1) = x_i(k) + \tau v_i(k) + \frac{\tau^2}{2} u_i(k)$, $v_i(k+1) = v_i(k) + \tau u_i(k)$, $\forall\, i = 1, \ldots, n$. In what follows, we call u_i *admissible* if it satisfies the constraint (6), i.e., $a_{\min} \leq u_i \leq a_{\max}$.

To characterize the constraint set, define the following real-valued functions at each time k, :

$$g_1(u_1(k)) := L + r \cdot v_1(k+1) - \frac{(v_1(k+1) - v_{\min})^2}{2a_{\min}} - \big[x_0(k+1) - x_1(k+1)\big], \tag{9}$$

and for each $i = 2, \ldots, n$,

$$g_i(u_{i-1}(k), u_i(k)) := L + r \cdot v_i(k+1) - \frac{(v_i(k+1) - v_{\min})^2}{2a_{\min}} - \big[x_{i-1}(k+1) - x_i(k+1)\big], \tag{10}$$

where $x_i(k+1)$ and $v_i(k+1)$ are expressed in terms of $u(k)$ as shown in (1). By slightly abusing notation, we write the above functions as $g_i(u(k))$ or $g_i(u)$ for each $i = 1, \ldots, n$. It is easy to verify that each g_i is a convex quadratic function. In

fact, $g_i(u) = \frac{1}{2}u^T E_i u + h_i^T u + \varphi_i$, $\forall\, i = 1, \ldots, n$, where h_i is a vector, φ_i is a scalar, and E_i is a positive semidefinite diagonal matrix, i.e.,

$$E_i = \operatorname{diag}\Big(\underbrace{0, \ldots, 0}_{(i-1)\ \text{copies}}, \ -\frac{\tau^2}{a_{\min}}, \ 0, \ldots, 0 \Big) \in \mathbb{R}^{n\times n}. \tag{11}$$

Therefore, given $(x_i(k), v_i(k))_{i=1}^n$ and $u_0(k)$, the constraint set for the control $u(k)$ is

$$\begin{aligned}\mathcal{P}((x_i(k), v_i(k))_{i=0}^n, u_0(k)) := \Big\{ u \in \mathbb{R}^n \,|\, & a_{\min} \le u_i \le a_{\max}, \ v_{\min} \le v_i(k) + \tau u_i \le v_{\max}, \\ & g_i(u) \le 0, \ \forall\, i = 1, \ldots, n \Big\} \subset \mathbb{R}^n. \end{aligned} \tag{12}$$

Consequently, for each $k \in \mathbb{Z}_+$, the optimization problem (5) can be written as

$$\text{minimize} \quad J(u(k)) \quad \text{subject to} \quad u(k) \in \mathcal{P}((x_i(k), v_i(k))_{i=0}^n, u_0(k)). \tag{13}$$

Remark 3.1. The constrained optimization problem in (5) can be viewed as a one-horizon model predictive control (MPC) problem subject to inequality constraints. The general MPC framework has been introduced for car following of a vehicle platoon (Dunbar and Caveney, 2012; Dunbar and Murray, 2006; Franco et al., 2008; Keviczky et al., 2006; Li et al., 2011; Wang et al., 2014; Zheng et al., 2016a). This study uses one-horizon model for two reasons. First, the general p-horizon MPC framework requires accurate prediction of the leading vehicle's movement in future time, which may be difficult to obtain in practice since the leading vehicle is subject to various unknown disturbances in a real-world traffic environment. Second, the general p-horizon MPC problem need extensive computation and is numerically more involved when p is large; its distributed computation is more sophisticated and need further investigation for real-time implementation. Nevertheless, extending the current formulation to the general MPC via distributed computation will be a future research topic.

3.1. Sequential feasibility and properties of the constraint set

It is noted from (13) that the constraint set of the underlying optimization problem (13) depends on the position and speed of the vehicles from its past time. A fundamental question for the optimization problem (13) is whether it is feasible at each time. We show below that the optimization problem (13) is *sequentially feasible*, namely, if $\mathcal{P}((x_i(k), v_i(k))_{i=0}^n, u_0(k))$ is nonempty at the initial time $k = 0$ and $(u_0(k), v_0(k))$ satisfy (6)–(7) for all $k \in \mathbb{Z}_+$, then the optimization problem (13) is feasible at each k along a system trajectory. For this purpose, we introduce the following functions for given $(x_s, v_s)_{s=0}^n$ where s denotes the vehicle index:

$$p_i((x_s, v_s)_{s=0}^n) := x_{i-1} - x_i - \left[L + r \cdot v_i - \frac{(v_i - v_{\min})^2}{2a_{\min}} \right], \qquad \forall\ i = 1, \ldots, n, \tag{14}$$

where each p_i characterizes dependence of the safety distance between two adjacent vehicles on their current position and speed. To simplify notation, we also write $p_i((x_s, v_s)_{s=0}^n)$ as p_i in the subsequent development.

Lemma 3.1. *Suppose $(x_s, v_s)_{s=0}^n$ and u_0 are given such that $a_{\min} \le u_0 \le a_{\max}$, $v_{\min} \le v_0 + \tau u_0 \le v_{\max}$, $v_{\min} \le v_i \le v_{\max}$ and $p_i((x_s, v_s)_{s=0}^n) \ge 0, \forall\, i = 1, \ldots, n$. Then the constraint set $\mathcal{P}((x_s, v_s)_{s=0}^n, u_0)$ is nonempty and convex.*

Proof. For notational simplicity, we write $\mathcal{P}((x_s, v_s)_{s=0}^n, u_0)$ as $\mathcal{P}$ in the following proof. For each given v_i satisfying $v_{\min} \le v_i \le v_{\max}$, define the continuous function $q_i : \mathbb{R} \to \mathbb{R}$ as

$$q_i(w) := v_i + \frac{\tau w}{2} + r \cdot w - \frac{w}{a_{\min}}\big[v_i - v_{\min}\big] - \frac{\tau w^2}{2a_{\min}}, \qquad \forall\ i = 1, \ldots, n. \tag{15}$$

We claim that if $v_{\min} < v_i \le v_{\max}$, then there exists $\widehat{u}_i$ with $a_{\min} < \widehat{u}_i < a_{\max}$ such that $v_{\min} < v_i + \tau\widehat{u}_i < v_{\max}$, and $q_i(\widehat{u}_i) < v_{\min}$. To show this claim, consider two cases as follows:

(1) $v_i + \tau a_{\min} \ge v_{\min}$. In this case, since $\tau a_{\min} < 0$, we have $v_{\min} \le v_i + \tau a_{\min} < v_i \le v_{\max}$, and $q_i(a_{\min}) = r \cdot a_{\min} + v_{\min} < v_{\min}$. Let $\widehat{u}_i := a_{\min} + \varepsilon$ for a sufficiently small $\varepsilon > 0$. By the continuity of q_i, we obtain $a_{\min} < \widehat{u}_i < a_{\max}$, $v_{\min} < v_i + \tau\widehat{u}_i < v_{\max}$, and $q_i(\widehat{u}_i) < v_{\min}$.

(2) $v_i + \tau a_{\min} < v_{\min}$ and $v_i > v_{\min}$. Let $u_i' := \frac{v_{\min} - v_i}{\tau} < 0$, which yields $v_i + \tau u_i' = v_{\min}$. It follows from $v_i + \tau a_{\min} < v_{\min}$ that $0 < \frac{u_i'}{a_{\min}} < 1$. Hence $a_{\min} < u_i' < a_{\max}$. By virtue of $v_i = v_{\min} - \tau u_i'$, $u_i' < 0$, $r \ge \tau$, and $v_i \ge v_{\min}$, we have

$$\begin{aligned} q_i(u_i') &= v_{\min} + \big[r - \tau\big]u_i' - \frac{u_i'}{a_{\min}}\big[v_i - v_{\min}\big] + \left(\frac{\tau u_i'}{2} - \frac{\tau (u_i')^2}{2a_{\min}} \right) \\ &\le v_{\min} + \frac{\tau u_i'}{2}\left(1 - \frac{u_i'}{a_{\min}} \right) < v_{\min}. \end{aligned}$$

Letting $\widehat{u}_i := u_i' + \varepsilon$ for a sufficiently small $\varepsilon > 0$, we have $a_{\min} < \widehat{u}_i < a_{\max}$, $v_{\min} < v_i + \tau\widehat{u}_i < v_{\max}$, and $q_i(\widehat{u}_i) < v_{\min}$.

This completes the proof of the claim. Furthermore, if $v_i = v_{\min}$, then by letting $\widehat{u}_i := 0$, we have $q_i(\widehat{u}_i) = v_{\min}$ and $v_i + \tau\widehat{u}_i = v_{\min}$.

Consider the $\widehat{u}_i$'s obtained above. Clearly, each $\widehat{u}_i$ is admissible, i.e., $\widehat{u}_i \in [a_{\min}, a_{\max}]$, and $\widetilde{v}_i := v_i + \tau\widehat{u}_i$ satisfies $v_{\min} \le \widetilde{v}_i \le v_{\max}$. Define $\widetilde{x}_i := x_i + \tau v_i + \frac{\tau^2}{2}\widehat{u}_i$ for each $i = 1, \dots, n$. By the assumptions on $(x_s, v_s)_{s=0}^n$ and u_0 and the definition of p_i, we verify the safety distant constraint for each $i = 1, \dots, n$ as follows:

$$
\begin{aligned}
&\widetilde{x}_{i-1} - \widetilde{x}_i - \left[L + r\cdot\widetilde{v}_i - \frac{(\widetilde{v}_i - v_{\min})^2}{2a_{\min}}\right] \qquad (16)\\
&= x_{i-1} - x_i - \left[L + r\cdot v_i - \frac{(v_i - v_{\min})^2}{2a_{\min}}\right] + \left\{\tau\left[v_{i-1} - v_i\right] + \frac{\tau^2}{2}\left[\widehat{u}_{i-1} - \widehat{u}_i\right]\right.\\
&\qquad \left. -\tau\cdot r\cdot\widehat{u}_i + \tau\frac{\widehat{u}_i}{a_{\min}}\left[v_i - v_{\min}\right] + \tau^2\frac{\widehat{u}_i^2}{2a_{\min}}\right\}\\
&= p_i + \tau\left\{\left[v_{i-1} - v_i\right] + \frac{\tau}{2}\left[\widehat{u}_{i-1} - \widehat{u}_i\right] - r\cdot\widehat{u}_i + \frac{\widehat{u}_i}{a_{\min}}\left[v_i - v_{\min}\right] + \tau\frac{\widehat{u}_i^2}{2a_{\min}}\right\}\\
&\ge \tau\left\{v_{i-1} + \frac{\tau}{2}\widehat{u}_{i-1} - \left[v_i + \frac{\tau}{2}\widehat{u}_i + r\cdot\widehat{u}_i - \frac{\widehat{u}_i}{a_{\min}}\left[v_i - v_{\min}\right] - \tau\frac{\widehat{u}_i^2}{2a_{\min}}\right]\right\}\\
&= \tau\left\{\frac{v_{i-1} + \widetilde{v}_{i-1}}{2} - q_i(\widehat{u}_i)\right\} \ge \tau\left\{v_{\min} - q_i(\widehat{u}_i)\right\}\\
&\ge 0,
\end{aligned}
$$

where the second-to-last inequality follows from $\widetilde{v}_i \ge v_{\min}, \forall\, i = 0, 1, \dots, n$ and $v_{i-1} + \frac{\tau}{2}\widehat{u}_{i-1} = \frac{v_{i-1} + v_{i-1} + \tau\widehat{u}_{i-1}}{2} = \frac{v_{i-1} + \widetilde{v}_{i-1}}{2} \ge v_{\min}$ for the given u_0 and the chosen $\widehat{u}_1, \dots, \widehat{u}_n$. This implies that $g_1(\widehat{u}_1) \le 0$ and $g_i(\widehat{u}_{i-1}, \widehat{u}_i) \le 0, \forall\, i = 2, \dots, n$. Consequently, $\widehat{u} := (\widehat{u}_1, \dots, \widehat{u}_n)^T \in \mathcal{P}$, and $\mathcal{P}$ is nonempty. Finally, since $g_i(u)$ defined in (9) and (10) are convex quadratic functions and the other constraints are polyhedral, we deduce that $\mathcal{P}$ is convex. □

Another basic question is under what conditions, the constraint set $\mathcal{P}((x_s, v_s)_{s=0}^n, u_0)$ has nonempty interior. This interior property is crucial to the Slater's constraint qualification which is essential to the development of distributed algorithms for solving the optimization problem (13). To address this question, we first establish Lemma 3.2 below, which states that the ith vehicle has a unique feasible u_i (which can be shown to be zero) if and only if all its preceding vehicles satisfy the tight safety distance bound (i.e., $p_j = 0$ for all $j = 1, \dots, i$) and move at the minimum speed (i.e., $v_j = v_{\min}$ for all $j = 0, 1, \dots, i$). Its proof is given in Appendix (cf. Section A.1).

Lemma 3.2. *Suppose $(x_s, v_s)_{s=0}^n$ and u_0 are given such that $a_{\min} \le u_0 \le a_{\max}$, $v_{\min} \le v_0 + \tau u_0 \le v_{\max}$, $v_{\min} \le v_i \le v_{\max}$ and $p_i((x_s, v_s)_{s=0}^n) \ge 0, \forall\, i = 1, \dots, n$. Then the following hold:*

(1) *Fix $i \in \{1, \dots, n\}$, the following two statements are equivalent:*
   (i) *$p_1 = \cdots = p_i = 0$, $v_0 = v_1 = \cdots = v_i = v_{\min}$, and $u_0 = u_1 = \cdots = u_i = 0$ for any $u = (u_1, \dots, u_n) \in \mathcal{P}((x_s, v_s)_{s=0}^n, u_0)$;*
   (ii) *there exists a constant $\psi \in [a_{\min}, a_{\max}]$ such that $u_i = \psi$ for any $u = (u_1, \dots, u_n) \in \mathcal{P}((x_s, v_s)_{s=0}^n, u_0)$, and such the constant $\psi = 0$;*

(2) *If $u_0 = 0$ and $\ell \in \{1, \dots, n\}$ is the largest index such that $p_1 = \cdots = p_\ell = 0$ and $v_0 = v_1 = \cdots = v_\ell = v_{\min}$, then $u_1 = \cdots = u_\ell = 0$ for any $u = (u_1, \dots, u_n) \in \mathcal{P}((x_s, v_s)_{s=0}^n, u_0)$, and there exist $\widehat{u}_{\ell+1}, \dots, \widehat{u}_n$ and a constant $\varepsilon > 0$ such that for any $u_j \in (\widehat{u}_j - \varepsilon, \widehat{u}_j + \varepsilon)$ with $j = \ell + 1, \dots, n$, $(0, \dots, 0, u_{\ell+1}, \dots, u_n) \in \mathcal{P}((x_s, v_s)_{s=0}^n, u_0)$.*

With the help of Lemma 3.2, the next proposition shows that any constraint set $\mathcal{P}((x_s, v_s)_{s=0}^n, u_0)$ takes exactly one of the three forms: it is either of nonempty interior, or singleton, or a Cartesian product of two convex sets, one of which is singleton and the other has nonempty interior.

Proposition 3.1. *Suppose $(x_s, v_s)_{s=0}^n$ and u_0 are given such that $a_{\min} \le u_0 \le a_{\max}$, $v_{\min} \le v_0 + \tau u_0 \le v_{\max}$, $v_{\min} \le v_i \le v_{\max}$ and $p_i((x_s, v_s)_{s=0}^n) \ge 0, \forall\, i = 1, \dots, n$. Then exactly one of the following holds for the constraint set $\mathcal{P}((x_s, v_s)_{s=0}^n, u_0) \subset \mathbb{R}^n$:*

(1) *$\mathcal{P}((x_s, v_s)_{s=0}^n, u_0)$ has nonempty interior;*
(2) *There exist $1 \le \ell \le n-1$ and a convex set $\mathcal{P}' \subset \mathbb{R}^{n-\ell}$ with nonempty interior such that $\mathcal{P}((x_s, v_s)_{s=0}^n, u_0) = \{(u_1, \dots, u_\ell, u_{\ell+1}, \dots, u_n) \,|\, u_1 = \cdots = u_\ell = 0, \quad (u_{\ell+1}, \dots, u_n) \in \mathcal{P}'\}$;*
(3) *$\mathcal{P}((x_s, v_s)_{s=0}^n, u_0)$ contains the zero vector only.*

In particular, if $v_0 > v_{\min}$, then $\mathcal{P}((x_s, v_s)_{s=0}^n, u_0)$ has nonempty interior.

Proof. This result follows from Lemma 3.2. Specifically, (i) if $u_0 > 0$ or the index ℓ specified in statement (2) of Lemma 3.2 does not exist, then $\mathcal{P}((x_s, v_s)_{s=0}^n, u_0)$ has nonempty interior; (ii) if $u_0 = 0$ and the index ℓ specified in statement (2) of Lemma 3.2 satisfies $1 \le \ell \le n-1$, then $\mathcal{P}((x_s, v_s)_{s=0}^n, u_0)$ is of the stated form in condition (2); (iii) if $u_0 = 0$

and $\ell = n$, then $\mathcal{P}((x_s, v_s)_{s=0}^n, u_0) = \{0\}$. Finally, if $v_0 > v_{\min}$, then the index ℓ specified in statement (2) of Lemma 3.2 does not exist such that $\mathcal{P}((x_s, v_s)_{s=0}^n, u_0)$ has nonempty interior. □

We give a physical interpretation of the three cases in the above proposition. Case (1) corresponds to the situation where the leading vehicle is accelerating or not all of its following vehicles satisfy the tight safety distance bounds and move at the minimum speed. In this case, any u' perturbed from a feasible u remains feasible as long as a perturbation is small enough. Case (3) corresponds to the situation where the leading vehicle has zero acceleration, all vehicles move at the minimum speed, and each following vehicle satisfies the tight safety distance bound. In this case, the only feasible u is the zero acceleration. The remaining case is Case (2), where the leading vehicle has zero acceleration, the first ℓ following vehicles satisfy the tight safety distance bounds and move at the minimum speed, but the rest $(n-\ell)$ vehicles do not. Thus for the latter vehicles, any u' perturbed from a feasible u remains feasible under small perturbations.

3.2. Existence and uniqueness of optimal solution

For notational simplicity, we denote $\mathcal{P}((x_s, v_s)_{s=0}^n, u_0)$ by $\mathcal{P}$ in the subsequent development unless we want to emphasize its dependence on $(x_s, v_s)_{s=0}^n$ and u_0.

Proposition 3.2. *Suppose $(x_s, v_s)_{s=0}^n$ and u_0 are given such that $a_{\min} \le u_0 \le a_{\max}$, $v_{\min} \le v_0 + \tau u_0 \le v_{\max}$, $v_{\min} \le v_i \le v_{\max}$ and $p_i((x_s, v_s)_{s=0}^n) \ge 0, \forall i = 1, \dots, n$. Then the convex optimization problem: $\min J(u)$ subject to $u \in \mathcal{P}((x_s, v_s)_{s=0}^n, u_0)$ attains a unique optimal solution.*

Proof. It follows from (2) and (4) that the objective function J is quadratic, i.e., $J(u) := \frac{1}{2}u^T H u + c^T u + \gamma$, where the symmetric matrix $H := S^{-T}[\frac{\tau^4}{4}Q_z + \tau^2 Q_{z'}]S^{-1} + \tau^2 I$, and $c \in \mathbb{R}^n$ and $\gamma \in \mathbb{R}$ depend on τ, u_0 and $(x_s, v_s)_{s=0}^n$. Clearly, H is positive definite such that J is strongly (and thus strictly) convex. Hence the underlying optimization problem can be written as:

$$\begin{array}{ll} \text{minimize} & J(u) := \frac{1}{2}u^T H u + c^T u + \gamma, \\ \text{subject to} & a_{\min} \le u_i \le a_{\max}, \quad v_{\min} \le v_i + \tau u_i \le v_{\max}, \quad g_i(u) \le 0, \quad \forall i = 1, \dots, n. \end{array} \tag{17}$$

By Lemma 3.1, the constraint set $\mathcal{P}$ is nonempty and convex. Besides $\mathcal{P}$ is closed as it is defined by continuous functions. In view of the constraint conditions $a_{\min} \le u_i \le a_{\max}, \forall i = 1, \dots, n$, $\mathcal{P}$ is bounded and thus compact. By the continuity of $J(\cdot)$, the optimization problem (17) has an optimal solution. Since J is strictly convex and $\mathcal{P}$ is a convex set, that optimal solution is unique. □

The next result follows directly from Proposition 3.2 and induction on k; its proof is omitted.

Theorem 3.1. *Suppose $(x_s(0), v_s(0))_{s=0}^n$ and $u_0(k)$ are such that $a_{\min} \le u_0(k) \le a_{\max}, \forall k \in \mathbb{Z}_+$, $v_{\min} \le v_0(0) + \tau u_0(0) \le v_{\max}$, $v_{\min} \le v_i(0) \le v_{\max}$ and $p_i((x_s(0), v_s(0))_{s=0}^n) \ge 0, \forall i = 1, \dots, n$. Then for each $k \in \mathbb{Z}_+$, the constraint set $\mathcal{P}((x_s(k), v_s(k))_{s=0}^n, u_0(k))$ is nonempty, and the optimization problem (13) has a unique optimal solution $u_*(k)$.*

Remark 3.2. At each time $k \in \mathbb{Z}_+$, the optimal $u_*(k)$ is a function of $(x_s(k), v_s(k))_{s=0}^n$ and $u_0(k)$. Due to the structure of the objective function and state and control coupled constraints (e.g., the safety distance constraints), each component of $u_*(k)$ depends not only on the position and speed of its corresponding vehicle but also on those of the other vehicles. Hence, the proposed control scheme requires that each vehicle communicates to all the other vehicles, and the global information structure is used. Such the global information structure is suitable for a well-connected platoon. There has been a surging interest in car-following control under different communication topologies and local information structures (Desjardins and Chaib-draa, 2011; Li et al., 2015; Lin et al., 2012; Schakel et al., 2010; Wang et al., 2014; Zheng et al., 2016a; 2016b). We will consider local information structures in future research.

The optimization problem (17) is a convex quadratically constrained quadratic program, and can be solved via semidefinite program. But its algorithm requires centralized computation, which is not suitable for a large platoon. We develop distributed algorithms in the next section.

4. Distributed algorithms for constrained optimization problem

We study distributed algorithms for solving the constrained convex optimization problem (17) (or (13) at each k). By Proposition 3.1, we only need to consider the nontrivial constraint set $\mathcal{P}$ in Cases (1) and (2) shown in Proposition 3.1. To treat these two cases in a unified framework, we note that Case (2) can be reduced to Case (1). In fact, define $u' := (u_{\ell+1}, \dots, u_n)^T \in \mathbb{R}^{n-\ell}$ and the new objective function $J'(u') := J(0, \dots, 0, u_{\ell+1}, \dots, u_n)$, which is positive definite. Then the problem (17) reduces to a convex quadratically constrained quadratic program on $\mathbb{R}^{n-\ell}$:

$$\text{minimize} \quad J'(u') \qquad \text{subject to} \quad u' \in \mathcal{P}', \tag{18}$$

where the constraint set $\mathcal{P}'$ given below is nonempty, convex, and compact with nonempty interior:

$$\mathcal{P}' := \{u' \in \mathbb{R}^{n-\ell} \mid a_{\min} \le u_i \le a_{\max}, \ v_{\min} \le v_i + \tau u_i \le v_{\max}, \ g_i(u') \le 0, \ \forall i = \ell+1, \dots, n\}.$$

Clearly, the reduced optimization problem (18) has the same form as the problem (17) in Case (1). Particularly it has a unique optimal solution and satisfies the Slater's constraint qualification. Due to this reason, we consider Case (1) throughout this section; its results can be easily extended to Case (2) via the reduction described above.

4.1. Primal-dual formulation and optimality conditions

The optimization problem (17) can be formulated as the multiuser optimization problem (Koshal et al., 2011):

$$\begin{array}{ll} \text{minimize} & J(u) := \frac{1}{2}u^T H u + c^T u + \gamma, \\ \text{subject to} & \begin{cases} u_i \in \mathcal{X}_i, & \forall\, i = 1, \ldots, n, \\ g_i(u) \le 0, & \forall\, i = 1, \ldots, n, \end{cases} \end{array} \tag{19}$$

where each $\mathcal{X}_i := \{z \in \mathbb{R} \,|\, a_{\min} \le z \le a_{\max},\ \ v_{\min} \le v_i + \tau z \le v_{\max}\}$. Clearly, each $\mathcal{X}_i$ is a convex compact interval on $\mathbb{R}$ given by $\mathcal{X}_i = \{z \in \mathbb{R} \,|\, \max(a_{\min}, (v_{\min} - v_i)/\tau) \le z \le \min(a_{\max}, (v_{\max} - v_i)/\tau)\}$. Furthermore, each g_i is a convex quadratic function, and the gradient $\nabla J(u)$ is a linear function, and thus Lipschitz continuous, on $\mathbb{R}^n$.

Let the function $g : \mathbb{R}^n \to \mathbb{R}^n$ be $g(u) := (g_1(u), \ldots, g_n(u))^T$. The Lagrangian function corresponding to (19) is given by

$$\mathcal{L}(u, \lambda) := J(u) + \lambda^T g(u),$$

where $\lambda \in \mathbb{R}^n_+$ is the multiplier. Letting $\mathcal{X} := \mathcal{X}_1 \times \cdots \times \mathcal{X}_n \subset \mathbb{R}^n$, the primal problem for (19) is $\mathbf{P}: \inf_{u\in\mathcal{X}} \sup_{\lambda\in\mathbb{R}^n_+} \mathcal{L}(u, \lambda)$, and the associated dual problem is $\mathbf{D}: \sup_{\lambda\in\mathbb{R}^n_+} \inf_{u\in\mathcal{X}} \mathcal{L}(u, \lambda)$.

It follows from the Slater's constraint qualification and the existence of a unique optimal solution u_* to (19) that the strong duality holds such that the dual problem has a (possibly non-unique) optimal solution λ_*. This shows that $(u_*, \lambda_*) \in \mathcal{X} \times \mathbb{R}^n_+$ is a saddle point of the Lagrangian $\mathcal{L}(u, \lambda)$ on $\mathcal{X} \times \mathbb{R}^n_+$, i.e., for any $u \in \mathcal{X}$ and $\lambda \in \mathbb{R}^n_+$, $\mathcal{L}(u_*, \lambda) \le \mathcal{L}(u_*, \lambda_*) \le \mathcal{L}(u, \lambda_*)$. Let u' be an interior point of $\mathcal{P}$ such that $g_i(u') < 0$ for each i. By the saddle point relation described above, we have

$$\mathcal{L}(u', \lambda_*) \ge \mathcal{L}(u_*, \lambda_*) \ge \mathcal{L}(u_*, 0) = J(u_*) \ge \min_{u\in\mathbb{R}^n} J(u) = -\frac{c^T H^{-1} c}{2} + \gamma := \mu,$$

where the last equality follows from the fact that $J(\,\cdot\,)$ achieves its global minimum on $\mathbb{R}^n$ at $u = -H^{-1}c$. Therefore, for any $\lambda_* := (\lambda_{*,1}, \ldots, \lambda_{*,n})^T \in \mathbb{R}^n_+$, in view of $\mathcal{L}(u', \lambda_*) = J(u') + \sum_{i=1}^n \lambda_{*,i} \cdot g_i(u') \ge \mu$, we have $J(u') - \mu \ge \sum_{i=1}^n \lambda_{*,i} \cdot (-g_i(u')) \ge \lambda_{*,i} \cdot (-g_i(u'))$ for each $i = 1, \ldots, n$. Hence, the following (convex) box constraint set contains all dual optimal solutions λ_*:

$$\mathcal{D}' := \left\{ \lambda \in \mathbb{R}^n_+ \,|\, 0 \le \lambda_i \le \frac{J(u') - \mu}{-g_i(u')}, \quad \forall\, i = 1, \ldots, n \right\}.$$

This implies that the condition $\lambda \in \mathbb{R}^n_+$ in the primal and dual problems can be replaced by $\lambda \in \mathcal{D}'$. Thus a necessary and sufficient optimality condition is that (u_*, λ_*) satisfies the following Euclidean projection based nonsmooth equations for any positive constants ξ and θ (Koshal et al., 2011):

$$u_* = \Pi_{\mathcal{X}}\big(u_* - \xi \nabla_{u_i} \mathcal{L}(u_*, \lambda_*)\big), \qquad \lambda_* = \Pi_{\mathcal{D}'}\big(\lambda_* + \theta \nabla_\lambda \mathcal{L}(u_*, \lambda_*)\big), \tag{20}$$

where $\Pi_S(\,\cdot\,)$ is the Euclidean projection operator onto a closed convex set S, $\nabla_\lambda \mathcal{L}(u, \lambda) = g(u)$, and

$$\nabla_{u_i} \mathcal{L}(u, \lambda) = \frac{\partial J(u)}{\partial u_i} + \left(\frac{\partial g_1(u)}{\partial u_i}, \ldots, \frac{\partial g_n(u)}{\partial u_i} \right)^T \lambda = \Big(Hu + c + E_i u + h_i + h_{i+1} \Big)_i, \quad \forall\, i = 1, \ldots, n.$$

Let $\mathcal{I}_i$ denote the closed bounded interval $[0, \eta_i]$, where

$$\eta_i := \frac{J(u') - \mu}{-g_i(u')} \ge 0. \tag{21}$$

Since $\mathcal{X} = \mathcal{X}_1 \times \cdots \times \mathcal{X}_n$ and $\mathcal{D}' = \mathcal{I}_1 \times \cdots \times \mathcal{I}_n$ are box constraints, (20) is equivalent to

$$u_{*,i} = \Pi_{\mathcal{X}_i}\big(u_{*,i} - \xi \nabla_{u_i} \mathcal{L}(u_*, \lambda_*)\big), \qquad \lambda_{*,i} = \Pi_{\mathcal{I}_i}\big(\lambda_{*,i} + \theta g_i(u_*)\big), \qquad \forall\ i = 1, \ldots, n, \tag{22}$$

where $u_* := (u_{*,1}, \ldots, u_{*,n})^T$ and $\lambda_* := (\lambda_{*,1}, \ldots, \lambda_{*,n})^T$. Note that each $\mathcal{X}_i$ or $\mathcal{I}_i$ is an interval of the form $[a_i, b_i]$ for real numbers $a_i \le b_i$, and for any $z \in \mathbb{R}$,

$$\Pi_{[a_i, b_i]}(z) = \begin{cases} b_i, & \text{if } z \ge b_i \\ z, & \text{if } z \in [a_i, b_i] \\ a_i, & \text{if } z \le a_i \end{cases}$$

Since the Euclidean projections in (22) are decoupled, they can be computed in a decentralized manner and attain closed form solutions. This leads to distributed algorithms discussed below.

4.2. Dual based distributed algorithms

We consider dual and primal-dual based distributed algorithms in Koshal et al. (2009, 2011) to solve Eq. (20). Numerical experiments show that the original algorithms in Koshal et al. (2009, 2011) and their convergence analysis often lead to small step-lengths and slow convergence; see Section 6.2 for more explanation. To handle this problem, we modify these two algorithms or their convergence analysis to obtain larger step-lengths and faster numerical convergence. For instance, we use a different convergence argument for the dual based algorithm, and use the extra-gradient method for the primal-dual algorithm. It is also found via numerical tests that while the two (modified) distributed algorithms achieve the same numerical accuracy and convergence, the computation time of the dual based distributed algorithm is nearly half of that of the primal-dual algorithm. Hence, we focus on the dual based algorithm only as follows. For completeness, the primal-dual algorithm is given in Appendix (cf. Section A.2).

Let ε be a small positive number. The dual based regularized distributed algorithm consists of two sub-steps in each step: (i) for any given λ^m and u^m, solve the equation $u^{m+1} = \Pi_{\mathcal{X}}\big(u^{m+1} - \xi \nabla_u \mathcal{L}(u^{m+1}, \lambda^m)\big)$ using the following iteration with the step-length $\xi > 0$: $u^{m,0} := u^m$, and for each $s \in \mathbb{Z}_+$,

$$u_i^{m,s+1} = \Pi_{\mathcal{X}_i}\big(u_i^{m,s} - \xi \nabla_{u_i} \mathcal{L}(u^{m,s}, \lambda^m)\big), \qquad \forall\ i = 1, \ldots, n,$$

and (ii) once u^{m+1} is attained, compute λ^{m+1} as

$$\lambda_i^{m+1} = \Pi_{\mathcal{I}_i}(\lambda_i^m + \theta[g_i(u^{m+1}) - \varepsilon\lambda_i^m]), \qquad \forall\ i = 1, \ldots, n,$$

where $\theta > 0$ is the step-length for this sub-step. The pseudo code is given in Algorithm 1.

Algorithm 1 Dual based regularized distributed algorithm.

Choose a small $\varepsilon > 0$, and compute the positive constants $\mu_{\min}(H), M_g$;
Let $\theta := 2\mu_{\min}(H)/(M_g^2 + 2\varepsilon\mu_{\min}(H))$;
Initialize $m = 0$, and choose an initial vector $(u^0, \lambda^0) \in \mathcal{X} \times \mathcal{D}'$;
repeat
  Compute $L_u(\lambda^m)$ in (23), and let $\xi \in (0, 2/L_u(\lambda^m))$;
  Set $u^{m,0} := u^m$, and $s := 0$;
  repeat
    Perform distributed computation: $u_i^{m,s+1} \leftarrow \Pi_{\mathcal{X}_i}\big(u_i^{m,s} - \xi \nabla_{u_i} \mathcal{L}(u^{m,s}, \lambda^m)\big),\ \forall\ i = 1, \ldots, n$;
    $s \leftarrow s + 1$;
  until $\|u^{m,s} - u^{m,s-1}\|_2$ is sufficiently small
  Set $u^{m+1} \leftarrow u^{m,s}$;
  Perform distributed computation:$\lambda_i^{m+1} \leftarrow \Pi_{\mathcal{I}_i}\big(\lambda_i^m + \theta[g_i(u^{m+1}) - \varepsilon\lambda_i^m]\big),\ \forall\ i = 1, \ldots, n$;
  if $\lambda^{m+1} = \lambda^m$ **then**
    $(u_{*,\varepsilon}, \lambda_{*,\varepsilon}) \leftarrow (u^m, \lambda^m)$ and Stop;
  end if
  $m \leftarrow m + 1$;
until $\|\lambda^m - \lambda^{m-1}\|_2$ is sufficiently small
return (u^m, λ^m)

Next, for a symmetric matrix M, let $\mu_{\min}(M)$ and $\mu_{\max}(M)$ be its smallest and largest real eigenvalues respectively. To determine suitable step-lengths ξ and θ for a given $\varepsilon > 0$, we have:

(1) For a fixed $\lambda \in \mathcal{D}'$, $\nabla_u \mathcal{L}(u, \lambda) = \nabla J(u) + \sum_{i=1}^n \lambda_i \nabla g_i(u) = \big(H + \sum_{i=1}^n \lambda_i E_i\big)u + c + \sum_{i=1}^n \lambda_i h_i$ is strongly convex on $\mathcal{X}$ and is Lipschitz continuous on $\mathcal{X}$ with the Lipschitz constant

$$L_u(\lambda) := \mu_{\max}\left(H + \sum_{i=1}^n \lambda_i E_i\right). \tag{23}$$

It follows from (Polyak, 1987, Theorem 1 of Section 7.2) that if the positive step-length $\xi < 2/L_u(\lambda)$, then the sequence $(u^{m,s})$ generated by the above algorithm converges to u^{m+1} with the convergence rate given by $\max(|1 - \xi\mu_{\min}(H + \sum_{i=1}^n \lambda_i E_i)|, |1 - \xi L_u(\lambda)|)$.

(2) Let $u_*(\lambda)$ denote the solution to the equation $u = \Pi_{\mathcal{X}}\big(u - \xi \nabla_u \mathcal{L}(u, \lambda)\big)$ for a given λ. It follows from (Koshal et al., 2011, Lemma 4.1) that $-g(u_*(\lambda))$ is co-coercive in λ with the co-coercive constant $\mu_{\min}(H)/(M_g)^2$, where M_g is given in (32). Hence, if the step-length

$$\theta = \frac{2\mu_{\min}(H)}{M_g^2 + 2\varepsilon\mu_{\min}(H)},$$

then by (Koshal et al., 2011, Proposition 4.2), the sequence (λ^m) converges to the unique dual optimal solution $\lambda_{*,\varepsilon}$ with the convergence rate $1 - \theta\varepsilon$, namely, $\|\lambda^{m+1} - \lambda_{*,\varepsilon}\|_2 \le (1 - \theta\varepsilon)\|\lambda^m - \lambda_{*,\varepsilon}\|_2,\ \forall m \in \mathbb{Z}_+$.

5. Stability analysis for unconstrained closed-loop dynamics

This section studies the performance of the proposed control scheme and discusses how to choose penalty weights α_i's and β_i's to achieve the desired transient and asymptotic dynamics. Note that the proposed control scheme is generally nonlinear in state, particularly when the constraints are active. In this section, we focus on the case where the control is free of all the constraints, which leads to a linear closed-loop system as shown below, since this case is the most common and the most important scenario for a platoon. The results developed for this case will pave the way for future study of nonlinear dynamics under active constraints (Hu et al., 2010; Shen and Hu, 2012).

5.1. Linear closed-loop dynamics and stability analysis

We first establish a closed form solution of the optimal $u_*(k)$ from the optimization problem (5), assuming that all constraints are inactive. For this purpose, we see from (2) that

$$z(k+1) = z(k) + \tau z'(k) + \frac{\tau^2}{2} w(k), \qquad z'(k+1) = z'(k) + \tau w(k), \tag{24}$$

where $w_i(k) := u_{i-1} - u_i(k)$ for each $i = 1, \ldots, n$. Furthermore, $u(k) = -Sw(k) + u_0(k) \cdot \mathbf{1}$, where the matrix S is defined in (3). Recall that the penalty weights $\alpha := (\alpha_1, \ldots, \alpha_n)$ and $\beta := (\beta_1, \ldots, \beta_n)$ with $\alpha_i > 0$ and $\beta_i > 0$ for each i, and the diagonal matrices $D_\alpha := \mathrm{diag}(\alpha_1, \ldots, \alpha_n)$ and $D_\beta := \mathrm{diag}(\beta_1, \ldots, \beta_n)$; see Section 3 for details. At each time k, the objective function in (4) is

$$J(w(k)) = \frac{1}{2}\Big[z^T(k+1) Q_z z(k+1) + (z'(k+1))^T Q_{z'} z'(k+1)\Big] + \frac{\tau^2}{2} \| -Sw(k) + u_0(k)\mathbf{1}\|_2^2,$$

where $Q_z = P^T D_\alpha P$ and $Q_{z'} = P^T D_\beta P$. In view of (24) and $\| -Sw(k) + u_0(k)\mathbf{1}\|_2^2 = \big[-Sw(k) + u_0(k)\mathbf{1}\big]^T \big[-Sw(k) + u_0(k)\mathbf{1}\big]$, a straightforward computation shows that

$$\begin{aligned}\frac{\partial J}{\partial w(k)} &= \frac{\tau^2}{2} Q_z \Big[z(k) + \tau z'(k) + \frac{\tau^2}{2} w(k)\Big] + \tau Q_{z'} \Big[z'(k) + \tau w(k)\Big] + \tau^2 \Big(S^T S w(k) - u_0(k) S^T \mathbf{1}\Big) \\ &= \Big(\frac{\tau^4 Q_z}{4} + \tau^2 Q_{z'}\Big) w(k) + \frac{\tau^2 Q_z}{2} z(k) + \Big(\frac{\tau^3 Q_z}{2} + \tau Q_{z'}\Big) z'(k) + \tau^2 \Big(S^T S w(k) - u_0(k) S^T \mathbf{1}\Big).\end{aligned}$$

When the system is free of constraints, the optimal solution $w_*(k)$, which corresponds to the optimal $u_*(k)$ as shown in (3), is given by

$$\frac{\partial J}{\partial w(k)}\Big|_{w(k)=w_*(k)} = 0 \;\Leftrightarrow\; \Big(\frac{\tau^2 Q_z}{4} + Q_{z'} + S^T S\Big) w_*(k) + \frac{Q_z}{2} z(k) + \Big(\frac{\tau Q_z}{2} + \frac{Q_{z'}}{\tau}\Big) z'(k) - u_0(k) S^T \mathbf{1} = 0.$$

Since $S^T S$ is positive definite, so is $\frac{\tau^2 Q_z}{4} + Q_{z'} + S^T S$. Therefore, the optimal $w_*(k)$ is

$$w_*(k) = -\Big[\frac{\tau^2 Q_z}{4} + Q_{z'} + S^T S\Big]^{-1} \cdot \Big\{\frac{Q_z}{2} z(k) + \Big(\frac{\tau Q_z}{2} + \frac{Q_{z'}}{\tau}\Big) z'(k) - u_0(k) S^T \mathbf{1}\Big\}.$$

Define the matrix

$$W := \Big[\frac{\tau^2 Q_z}{4} + Q_{z'} + S^T S\Big]^{-1}. \tag{25}$$

Substituting $w_*(k)$ into the control system (2), we obtain the following linear dynamics for the closed-loop system on $\mathbb{R}^{2n}$:

$$\begin{bmatrix} z(k+1) \\ z'(k+1) \end{bmatrix} = \underbrace{\begin{bmatrix} I_n - \frac{\tau^2}{4} W Q_z & \tau I_n - W\Big(\frac{\tau^3}{4} Q_z + \frac{\tau}{2} Q_{z'}\Big) \\ -\frac{\tau}{2} W Q_z & I_n - W\Big(\frac{\tau^2}{2} Q_z + Q_{z'}\Big) \end{bmatrix}}_{A(\alpha,\beta,\tau)} \begin{bmatrix} z(k) \\ z'(k) \end{bmatrix} + \begin{bmatrix} \frac{\tau^2}{2} I_n \\ \tau I_n \end{bmatrix} W S^T \mathbf{1} \cdot u_0(k), \tag{26}$$

where $A(\alpha, \beta, \tau) \in \mathbb{R}^{2n \times 2n}$ with $\alpha = (\alpha_1, \ldots, \alpha_n)$ and $\beta = (\beta_1, \ldots, \beta_n)$.

Consider the matrix S in (3). Since the eigenvalues of $S^T S$ play an important role in stability and performance analysis, we discuss their properties below. Recall that $S^T S$ is positive definite, and $S^T S = P^T \Lambda P$ for an orthogonal matrix P and a diagonal matrix $\Lambda = \mathrm{diag}(s_1, \ldots, s_n)$ with $s_1 \geq s_2 \geq \cdots \geq s_n > 0$. Moreover, S^{-1} is lower triangular and $(S^T S)^{-1}$ is tridiagonal given by

$$S^{-1} = \begin{bmatrix} 1 & & & & \\ -1 & 1 & & & \\ & \ddots & \ddots & & \\ & & -1 & 1 & \\ & & & -1 & 1 \end{bmatrix}, \qquad (S^TS)^{-1} = \begin{bmatrix} 1 & -1 & & & \\ -1 & 2 & -1 & & \\ & \ddots & \ddots & \ddots & \\ & & -1 & 2 & -1 \\ & & & -1 & 2 \end{bmatrix}. \tag{27}$$

Lemma 5.1. *Let $n \geq 2$. The largest eigenvalue $\mu_{\max}(S^TS)$ satisfies $\frac{(n+1)(2n+1)}{6} \leq \mu_{\max}(S^TS) \leq \frac{n(n+1)}{2}$, and the smallest eigenvalue $\mu_{\min}(S^TS)$ satisfies $\frac{1}{4} \leq \mu_{\min}(S^TS) \leq \frac{1}{2}$.*

Proof. It is known that $0 < \mu_{\max}(S^TS) \leq \|S^TS\|_\infty$, where $\|S^TS\|_\infty$ is the ∞-norm of S^TS. It is easy to verify that $\|S^TS\|_\infty$ is the sum of the elements of the first row of S^TS given by $(n, n-1, \ldots, 1)$. Hence $\mu_{\max}(S^TS) \leq \|S^TS\|_\infty = \frac{n(n+1)}{2}$. Furthermore, $\mathbf{1}^TS^TS\mathbf{1} \leq \mu_{\max}(S^TS) \cdot \|\mathbf{1}\|_2^2$, where $\mathbf{1} := (1, \ldots, 1)^T \in \mathbb{R}^n$. Note that $\mathbf{1}^TS^TS\mathbf{1} = \sum_{k=1}^n k^2 = \frac{n(n+1)(2n+1)}{6}$ and $\|\mathbf{1}\|_2^2 = n$. This leads to the desired bounds for $\mu_{\max}(S^TS)$.

To show the bounds for $\mu_{\min}(S^TS)$, let $y = (y_1, \ldots, y_n)^T \in \mathbb{R}^n$ with $y_i = (-1)^i$ for each $i = 1, \ldots, n-1$, and $y_n = 1$ if n is even and $y_n = 0$ if n is odd. It can be shown that $y^TS^TSy = \frac{n}{2}$ if n is even, and $y^TS^TSy = \frac{n-1}{2}$ if n is odd. Since $y^TS^TSy \geq \mu_{\min}(S^TS)\|y\|_2^2$, we have $\mu_{\min}(S^TS) \leq \frac{1}{2}$. Finally, in light of the structure of $(S^TS)^{-1}$ given in (27), we deduce that $\mu_{\max}((S^TS)^{-1}) = \|(S^TS)^{-1}\|_2 \leq \sqrt{\|(S^TS)^{-1}\|_1 \cdot \|(S^TS)^{-1}\|_\infty} = \|(S^TS)^{-1}\|_\infty \leq 4$. Therefore, $\mu_{\min}(S^TS) = \frac{1}{\mu_{\max}((S^TS)^{-1})} \geq 1/4$. □

The next proposition establishes asymptotic stability of the linear closed-loop dynamics. Along with Lemma 5.1, it lays a ground for performance analysis of the linear closed-loop system.

Proposition 5.1. *Given any positive numbers τ and α_i, β_i for each $i = 1, \ldots, n$, the matrix $A(\alpha, \beta, \tau)$ is Schur stable, i.e., each eigenvalue $\mu \in \mathbb{C}$ of $A(\alpha, \beta, \tau)$ satisfies $|\mu| < 1$. Moreover, for any eigenvalue μ_i of $A(\alpha, \beta, \tau)$, there is a positive eigenvalue s_i of S^TS such that the following hold:*

(1) *if μ_i is non-real, then $|\mu_i|^2 = \frac{s_i}{d_i}$, where $d_i := \frac{\alpha_i\tau^2}{4} + \beta_i + s_i$;*

(2) *if μ_i is real, then $1 - (\frac{\alpha_i\tau^2}{2} + \beta_i)\frac{1}{d_i} < \mu_i < 1 - \frac{\alpha_i\tau^2}{4d_i}$.*

Proof. Fix positive numbers τ and $\alpha_i, \beta_i, \forall i = 1, \ldots, n$, and write $A(\alpha, \beta, \tau)$ as A for notational simplicity. We will convert the matrix A via a similarity transformation to a block diagonal matrix in (28) whose eigenvalues can be easily estimated. Since $S^TS = P^T\Lambda P$, $Q_z = P^TD_\alpha P$ and $Q_{z'} = P^TD_\beta P$, the matrix W in (25) becomes $W = P^T\mathrm{diag}(d_1, \ldots, d_n)^{-1}P$, where $d_i := \frac{\alpha_i\tau^2}{4} + \beta_i + s_i > 0$ for each $i = 1, \ldots, n$. Letting the diagonal matrix $D := \mathrm{diag}(d_1, \ldots, d_n)$, we obtain

$$\widehat{A} := \begin{bmatrix} P & 0 \\ 0 & P \end{bmatrix} \cdot A \cdot \begin{bmatrix} P^T & 0 \\ 0 & P^T \end{bmatrix} = \begin{bmatrix} I_n - D^{-1}\frac{\tau^2D_\alpha}{4} & \tau\left(I_n - D^{-1}\left(\frac{\tau^2D_\alpha}{4} + \frac{D_\beta}{2}\right)\right) \\ -D^{-1}\frac{\tau D_\alpha}{2} & I_n - D^{-1}\left(\frac{\tau^2D_\alpha}{2} + D_\beta\right) \end{bmatrix}.$$

Note that $\widehat{A}$ and A have exactly same eigenvalues. Let $\widetilde{z} := (z_1, z_1', z_2, z_2', \ldots, z_n, z_n')^T \in \mathbb{R}^{2n}$ for any $(z, z')^T = (z_1, \ldots, z_n, z_1', \ldots, z_n')^T \in \mathbb{R}^{2n}$. Since the coordination transformation $\widetilde{z} = E(z, z')^T$ is defined by an (invertible) permutation matrix $E \in \mathbb{R}^{2n\times 2n}$ (satisfying $E^{-1} = E^T$), we see that

$$\widehat{A} \cdot \begin{bmatrix} z \\ z' \end{bmatrix} = E^{-1} \underbrace{\begin{bmatrix} \widetilde{A}_1 & & & \\ & \widetilde{A}_2 & & \\ & & \ddots & \\ & & & \widetilde{A}_n \end{bmatrix}}_{\widetilde{A}} \cdot \widetilde{z}, \tag{28}$$

where $\widetilde{A} := E\widehat{A}E^T \in \mathbb{R}^{2n\times 2n}$ is a block diagonal matrix with each block $\widetilde{A}_i$ given by

$$\widetilde{A}_i := \begin{bmatrix} a_{11} & a_{12} \\ a_{21} & a_{22} \end{bmatrix} = \begin{bmatrix} 1 - \frac{\alpha_i\tau^2}{4d_i} & \tau\left(1 - \left(\frac{\alpha_i\tau^2}{4} + \frac{\beta_i}{2}\right)\frac{1}{d_i}\right) \\ -\frac{\alpha_i\tau}{2d_i} & 1 - \left(\frac{\alpha_i\tau^2}{2} + \beta_i\right)\frac{1}{d_i} \end{bmatrix} \in \mathbb{R}^{2\times 2}. \tag{29}$$

This shows that the set of all the eigenvalues of $\widehat{A}$ is the union of the eigenvalues of $\widetilde{A}_i$ for all i.

In what follows, we show that each $\widetilde{A}_i$ is Schur stable. Toward this end, consider two cases:

(1) $\widetilde{A}_i$ has a pair of complex eigenvalues $(\mu_i, \bar{\mu}_i)$. A straightforward computation yields

$$\det(\widetilde{A}_i) = \left[1 - \frac{\alpha_i\tau^2}{4d_i}\right] \cdot \left[1 - \frac{\frac{\alpha_i\tau^2}{2} + \beta_i}{d_i}\right] + \left[\tau\left(1 - \frac{\frac{\alpha_i\tau^2}{4} + \frac{\beta_i}{2}}{d_i}\right)\right] \cdot \frac{\alpha_i\tau}{2d_i} = 1 - \frac{\frac{\alpha_i\tau^2}{4} + \beta_i}{d_i} = \frac{s_i}{d_i},$$

where we use the fact that $d_i := \frac{\alpha_i\tau^2}{4} + \beta_i + s_i$. This implies that $0 < \det(\widetilde{A}_i) < 1$. Since $\det(\widetilde{A}_i) = \mu_i \cdot \bar{\mu}_i = |\mu_i|^2$, we have $|\mu_i| = |\bar{\mu}_i| < 1$.

(2) $\widetilde{A}_i$ has two real eigenvalues. Let $\mu \in \mathbb{R}$ be such an eigenvalue, and $v = (v_1, v_2)^T \in \mathbb{R}^2$ be its associated eigenvector. Recalling that a_{jk} denotes (j, k)-component of $\widetilde{A}_i$, we thus have

$$\widetilde{A}_i v = \mu \cdot v \implies \begin{cases} a_{11} v_1 + a_{12} v_2 = \mu v_1 \\ a_{21} v_1 + a_{22} v_2 = \mu v_2 \end{cases},$$

where $0 < a_{11} < 1$, $a_{21} < 0$ and $a_{12} > 0$ in view of $\frac{\alpha_i \tau^2}{4} + \frac{\beta_i}{2} < \frac{\alpha_i \tau^2}{4} + \beta_i < d_i$. This implies that both v_1 and v_2 are nonzero. Besides, by using $0 < \frac{\alpha_i \tau^2}{2} + \beta_i < 2d_i$, we have $-1 < a_{22} < 1$. It follows from the second equation that $v_1 = \frac{\mu - a_{22}}{a_{21}} v_2$. Substituting it into the first equation, we have $a_{12} v_2 = (\mu - a_{11}) \frac{\mu - a_{22}}{a_{21}} v_2$ and thus $a_{12} = (\mu - a_{11}) \frac{\mu - a_{22}}{a_{21}} > 0$. Since $a_{12} > 0$ and $a_{21} < 0$, we deduce that $(\mu - a_{11})(\mu - a_{22}) < 0$ such that $\min(a_{11}, a_{22}) < \mu < \max(a_{11}, a_{22})$. In particular, since $a_{11} \geq a_{22}$, we have $a_{22} < \mu < a_{11}$. Therefore, $|\mu| < \max(|a_{11}|, |a_{22}|) < 1$.

Consequently, A is Schur stable, and the desired bounds for an eigenvalue of A follow directly from the above argument. □

Remark 5.1. Since the eigenvalues of $A(\alpha, \beta, \tau)$ or $\widetilde{A}_i$ are crucial to both asymptotic stability and traffic transient dynamics, we discuss more of their properties using Proposition 5.1.

(1) As $0 < \det(\widetilde{A}_i) = \frac{s_i}{d_i} < 1$ for each i, every eigenvalue of $\widetilde{A}_i$ is nonzero. Further, if $\widetilde{A}_i$ has real eigenvalues $\mu_{i,1}$, $\mu_{i,2}$, then $\mu_{i,1}$ and $\mu_{i,2}$ must have the same sign. Moreover, in view of the trace of $\widetilde{A}_i$ given by $\mathrm{trace}(\widetilde{A}_i) = (\beta_i + 2s_i - \frac{\tau^2}{4}\alpha_i)/d_i$, we conclude that if $\beta_i + 2s_i \geq \frac{\tau^2}{4}\alpha_i$, then $\widetilde{A}_i$ has either a pair of non-real eigenvalues or a pair of positive eigenvalues.

(2) Since $\det(\widetilde{A}_i)$ is the product of two (possibly non-real) eigenvalues whose absolute values are less than one, we obtain the lower bound of an eigenvalue μ of $\widetilde{A}_i$: $|\mu| > \det(\widetilde{A}_i) = \frac{s_i}{d_i} \geq \frac{s_n}{\frac{\alpha_i \tau^2}{4} + \beta_i + s_n} \geq \frac{1}{\alpha_i \tau^2 + 4\beta_i + 1}$, where we use $s_i \geq s_n = \mu_{\min}(S^T S) \geq 1/4$. Furthermore, let μ be a positive eigenvalue of $\widetilde{A}_i$. Then it follows from Proposition 5.1 that $\frac{s_i}{d_i} < \mu < 1 - \frac{\alpha_i \tau^2}{4 d_i}$.

(3) It follows from Lemma 5.1 that $s_1 := \mu_{\max}(S^T S)$ satisfies $\frac{n^2}{3} \leq s_1 \leq \frac{n^2}{2}$ for any sufficiently large n. Hence if α_1 and β_1 are independent of n or are of order less than n^2, then as $n \to \infty$, some eigenvalue of $\widetilde{A}_1$ tends to 1, which leads to slow dynamic response.

5.2. Choice of penalty weights α_i's and β_i's

The penalty weights α_i's and β_i's in the objective function J in (4) can be chosen in different ways to achieve desired closed-loop performance. We describe two approaches as follows.

1. Choice of α_i's and β_i's based on desired eigenvalues of the linear closed-loop system. Suppose the eigenvalues of the linear closed-loop system (26) are given *a priori* based on desired performance, e.g., smooth transient dynamics and asymptotic dynamics. Let $\mu_{i,1}$, $\mu_{i,2}$ denote such a pair of (possibly complex) eigenvalues within the unit circle, i.e., $0 < |\mu_{i,1}| < 1$ and $0 < |\mu_{i,2}| < 1$. By the argument below (29), we have

$$\mu_{i,1} \cdot \mu_{i,2} = \det(\widetilde{A}_i) = \frac{s_i}{d_i}, \quad \mu_{i,1} + \mu_{i,2} = \mathrm{trace}(\widetilde{A}_i) = 1 - \frac{\alpha_i \tau^2}{4 d_i} + 1 - \left(\frac{\alpha_i \tau^2}{2} + \beta_i\right)\frac{1}{d_i} = \frac{s_i}{d_i} + 1 - \frac{\alpha_i \tau^2}{2 d_i},$$

where $d_i = \frac{\alpha_i \tau^2}{4} + \beta_i + s_i$. It follows from the first equation that $d_i = s_i / \det(\widetilde{A}_i)$. Substituting it into the second equation, we obtain

$$\mathrm{trace}(\widetilde{A}_i) = \det(\widetilde{A}_i) + 1 - \left(\frac{\tau^2 \det(\widetilde{A}_i)}{2 s_i}\right)\alpha_i \implies \alpha_i = \frac{2 s_i \cdot \left[\det(\widetilde{A}_i) + 1 - \mathrm{trace}(\widetilde{A}_i)\right]}{\tau^2 \det(\widetilde{A}_i)}.$$

Once α_i is attained, by using $d_i = s_i / \det(\widetilde{A}_i)$ and the definition of d_i, we further have

$$\beta_i = d_i - \left(\frac{\alpha_i \tau^2}{4} + s_i\right) = \frac{s_i}{\det(\widetilde{A}_i)} - \left(\frac{\alpha_i \tau^2}{4} + s_i\right).$$

The above results apply to each $\widetilde{A}_i$ with $i = 1, \ldots, n$. Since s_1 is of order n^2 (cf. Lemma 5.1), α_1 and β_1 will be of order n^2.

2. Empirical choice of α_i's and β_i's. We will avoid negative eigenvalues of $\widetilde{A}_i$, since such eigenvalues yield high-frequency oscillations. Hence, by (1) of Remark 5.1, we may choose $\beta_i + 2s_i \geq \frac{\tau^2}{4}\alpha_i$ or simply $\beta_i \geq \frac{\tau^2}{4}\alpha_i$. Moreover, in view of (2)-(3) of Remark 5.1 and Proposition 5.1, we expect α_i and β_i to be of order n^2, especially when the platoon size n is large. Such a choice leads to smaller eigenvalues and faster transient responses, but it requires large control inputs, which often yield control or speed saturation and other nonlinear effects that may worsen the closed-loop dynamics. Therefore, it is necessary to attain a tradeoff between fast dynamic response and mild control input by choosing moderate coefficients of the term n^2 in α_i and β_i. Motivated by these discussions, we consider the penalty weights of the following form:

$$\alpha_i = \kappa_i(\tau) \cdot n^2 - \varrho_i(n), \qquad \beta_i = \kappa_i' \cdot n^2 - \varrho_i'(n), \qquad \forall\, i = 1, \ldots, n, \tag{30}$$

where $\kappa_i(\tau) \in (0, 1)$ and $\kappa_i' \in (0, 1)$ are small positive coefficients of n^2, and ϱ_i and $\varrho_i'(n)$ are (positive) linear functions in n. In order to minimize traffic oscillations, we often put more penalty on $z'(k+1)$ in the objective function J. Hence κ_i' is typically larger than $\kappa_i(\tau)$ for each i.

6. Numerical experiments

6.1. Numerical experiment design and choice of control parameters

Numerical experiments are conducted to validate the applicability and efficiency of the proposed approaches in three aspects: (1) test numerical performance of the distributed algorithms; (2) test platoon performance under the proposed car-following control scheme, e.g., the capability of maintaining stable car-following distance and mitigating traffic oscillations; and (3) compare the performance of the proposed car-following scheme with a conventional CACC scheme in Schakel et al. (2010).

To reach these objectives, we consider a platoon of ten vehicles which consists of a leading vehicle labeled by 0 and nine following vehicles, i.e., $n = 9$. All vehicles in this platoon are considered as connected and autonomous vehicles. The leading vehicle is uncontrolled, but it may send real-time movement information, i.e., position, speed, and acceleration, to its following vehicles; the nine following vehicles are under control by the proposed car-following control scheme. We use the following physical parameters for the vehicles and constraints through experiments unless otherwise stated: the desired spacing $\Delta = 50$ m; the vehicle length $L = 5$ m; the acceleration and deceleration limits $a_{\max} = 1.35$ m/s^2 and $a_{\min} = -8$ m/s^2; the speed limits $v_{\max} = 27.78$ m/s and $v_{\min} = 0$ m/s; the sample time $\tau = 1$ s and the reaction time $r = \tau = 1$ s. The initial state of the platoon is $z_i(0) = \Delta = 50$ m and $v_i(0) = 25$ m/s for all $i = 1, \ldots, 9$, and the time length is 200 s. Given $n = 9$, $\tau = 1$ s, and other parameters, we apply (30) to find the penalty weights that determine the proposed control scheme. In particular, we choose the following penalty weights with $n = 9$:

$$\alpha_i = 0.1n^2 - 0.6(n+1-i), \quad \beta_i = 0.3n^2 - 1.2(n+1-i), \qquad i = 1, \ldots, n.$$

Based on the linear dynamic analysis in Section 5.1, all the eigenvalues of $A(\alpha, \beta, \tau)$ are positive or non-real within the unit circle: the smallest eigenvalue is 0.0120, the largest eigenvalue is 0.8901, and among the eighteen eigenvalues of $A(\alpha, \beta, \tau)$, ten eigenvalues have their absolute values between 0.8496 and 0.8901, and the other eight (real) eigenvalues are between 0.0120 and 0.2369.

Three scenarios are considered to evaluate the proposed car-following control scheme.

- **Scenario 1**: The leading vehicle performs instantaneous deceleration/acceleration and then keeps a constant speed for a while. The goal of this scenario is to test if the platoon can maintain stable spacing and speed when the leading vehicle is subject to acceleration or deceleration disturbances. The movement profile of the leading vehicle in this scenario is set as follows: the leading vehicle decelerates from $t = 51$ s to $t = 54$ s with the deceleration -2 m/s^2, and maintains a constant speed till $t = 100$ s. After that, it restores to its original speed 25 m/s with the acceleration 1 m/s^2.
- **Scenario 2**: The leading vehicle performs periodical acceleration/deceleration. The goal of this scenario is to test whether the proposed control scheme can reduce periodical spacing and speed fluctuation. The movement profile of the leading vehicle in this scenario is set as follows: the leading vehicle periodically changes its acceleration and deceleration from $t = 51$ s to $t = 100$ s with the period $T = 4$ s and acceleration/deceleration $\pm$ 1 m/s^2. Then it maintains its original constant speed 25 m/s after $t = 100$ s.
- **Scenario 3**: The motion of the leading vehicle is determined by real world trajectory data from an oscillating traffic flow. Specifically, we use NGSIM data on eastbound I-80 in San Francisco Bay area at Emeryville, California from 5:00 pm to 5:15 pm on April 13, 2005. The goal of this scenario is to test the performance of the proposed control scheme in a real traffic environment. Since the acceleration/deceleration of the leading vehicle is collected every 0.5 s in real-time, the sample time is set as $\tau = 0.5$ s. Further, the speed limit of a real road segment is $v_{\max} = 33.33$ m/s. The experiment setup of this scenario is chosen as follows: the desired spacing $\Delta = 55$ m, and $z_i(0) = 55$ m, $v_i(0) = 18.33$ m/s for each $i = 1, \ldots, n$, the time length is 45 s, and we use real trajectory data in an oscillating traffic flow for the leading vehicle's motion. Other parameters remain the same as before.

6.2. Computational performance of distributed algorithm

We apply the dual based regularized distributed algorithm (or DBR algorithm), i.e., Algorithm 1 in Section 4.2. We choose $\varepsilon = 0.1$ and the step-length $\theta = 0.0074$, and ξ is chosen from the interval [0.0254, 0.140] (depending on λ^m). Note that under the selected penalty weights, the matrix H in the objective function J has a high condition number which is approximately 100. Thus the step-lengths of the original dual and primal-dual algorithms given in Koshal et al. (2011) are almost 100 times smaller than the current choices, and they yield very slow convergence. This motivates us to apply the modified algorithms and different convergence analysis argument.

The distributed algorithm is implemented on MATLAB 7.1 and run on a computer with the following processor: Intel(R) Core(TM) $i7-3770$ CPU @ 3.40GHz and RAM: 8.0GB. We test the DBR algorithm in terms of numerical accuracy, convergence and efficiency. Figs. 1 and 2 show the numerical performance of the DBR algorithm for Scenario 1. The mean and variance

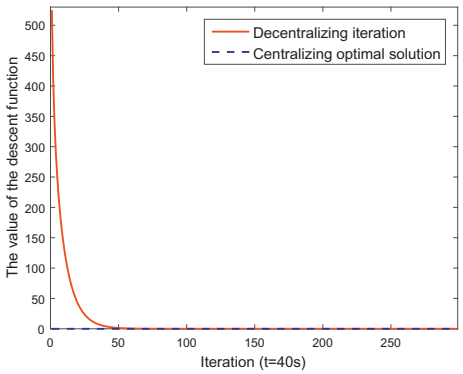

(a) $t = 40s$ (Stable state)

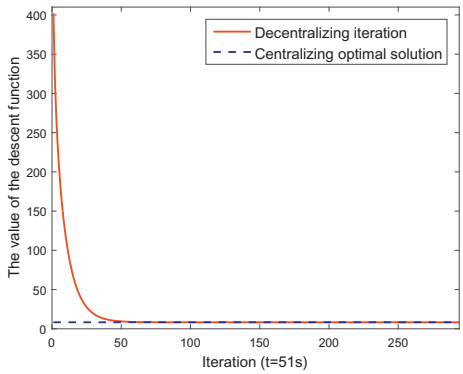

(b) $t = 51s$ (The leading vehicle decelerates)

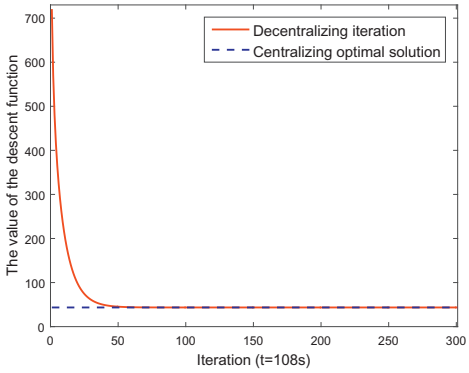

(c) $t = 108s$ (Most iterations)

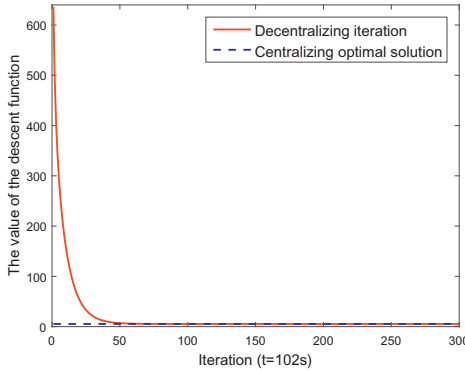

(d) $t = 102s$ (The leading vehicle accelerates)

Fig. 1. Illustration of the convergence of the DBR algorithm in Scenario 1.

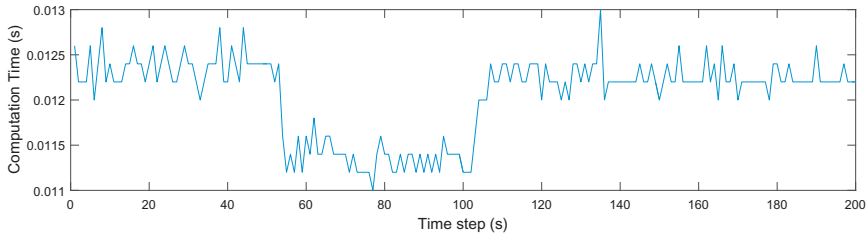

Fig. 2. Computation performance of the DBR algorithm in Scenario 1.

Table 1
The mean and variance of computation time and iterations for the DBR algorithm.

Scenarios	Computation time (s)		The number of iterations	
	Mean	Variance	Mean	Variance
1	0.0115	0.000388	297.91	0.9595
2	0.0114	0.000361	297.93	0.4540
3	0.0047	0.000390	109.34	1.1334

of computation time and iteration numbers of each step in Scenarios 1, 2 and 3 are presented in Table 1. It is shown in Fig. 1 that the objective function strictly decreases along numerical iterations in all the scenarios and converges to the result obtained from a centralized algorithm. Thus the DBR algorithm converges consistently in all scenarios. Moreover, it takes 0.011-0.013s to reach convergence in each scenario with 291–300 iterations (cf. Fig. 2). Hence we conclude that the numerical performance of the DBR algorithm is satisfactory, and the DBR algorithm is suitable for real-time computation.

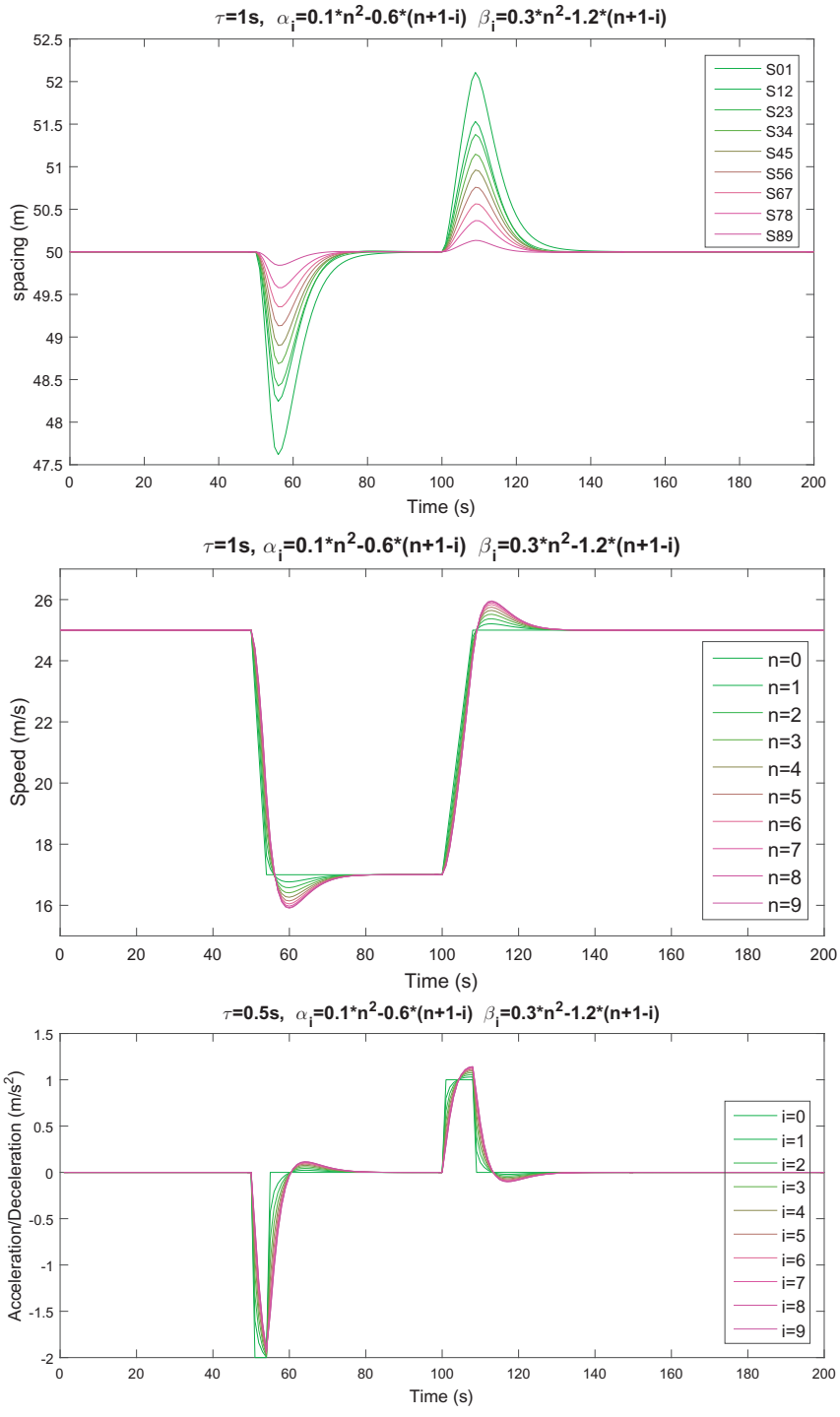

Fig. 3. Time history of spacing changes (top), vehicle speed (middle), and control input (bottom) in Scenario 1.

6.3. Performance of car-following control scheme

In this subsection, we discuss and evaluate the performance of the proposed car-following control scheme in the three scenarios. In each scenario, we focus on three performance criteria: the spacing between two adjacent vehicles denoted by $S_{i,i+1}(k) := z_i(k) + \Delta$, the vehicle speed $v_i(k)$, and the control input (or acceleration/deceleration) $u_i(k)$, for each i.

- **Scenario 1**. In this scenario, the leading vehicle performs instantaneous acceleration and deceleration. Fig. 3 displays the spacing changes in the platoon and shows that the spacing converges to the desired constant Δ under either accelera-

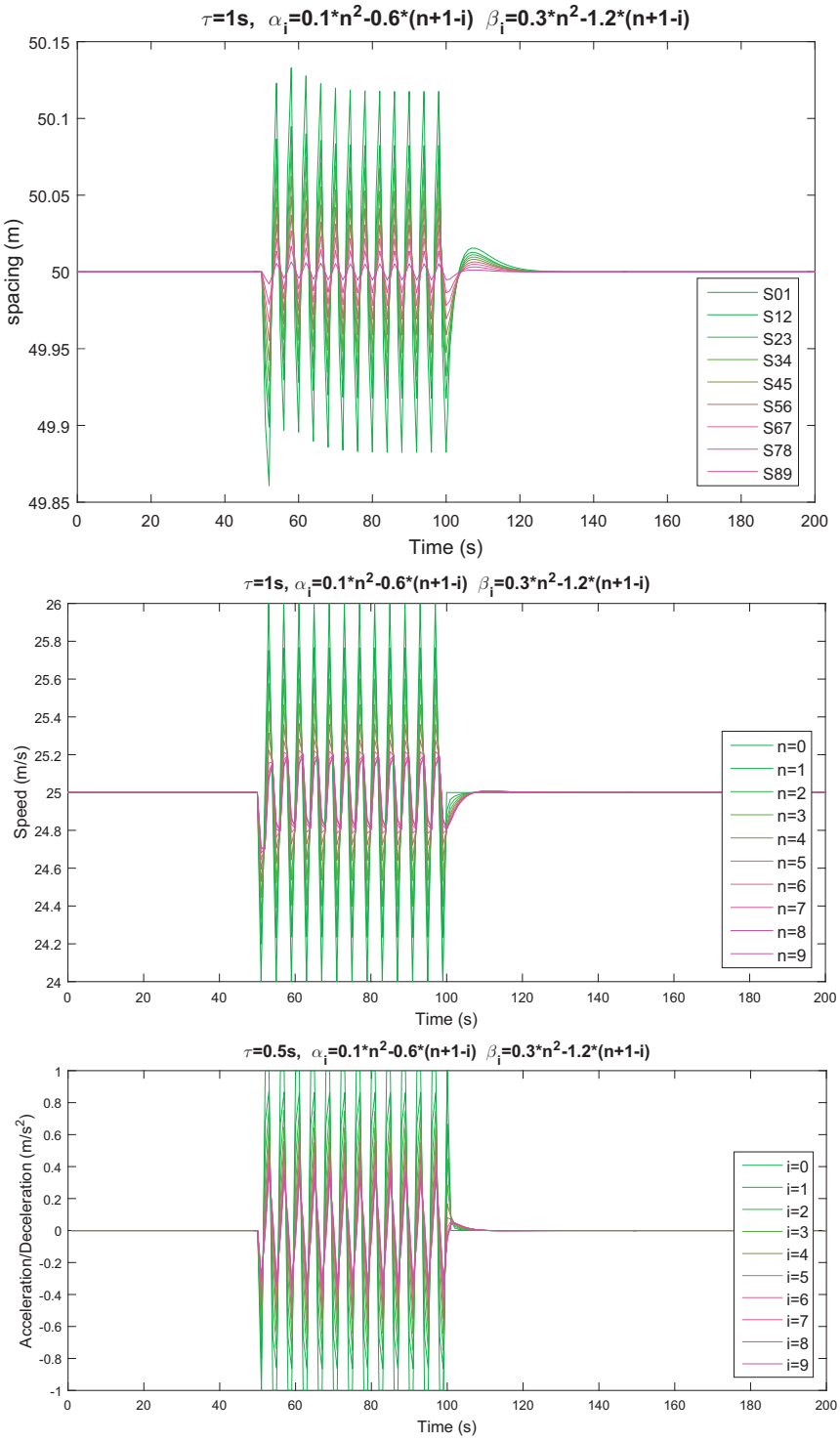

Fig. 4. Time history of spacing changes (top), vehicle speed (middle), and control input (bottom) in Scenario 2.

tion or deceleration disturbances. The plot also shows that it takes 38 s and 42 s to reach a steady state respectively. Moreover, the magnitude of spacing variations is decaying as the vehicle indices i increase. This indicates that the platoon becomes more stable when approaching its tail. For instance, the maximum spacing deviation between the first two vehicles (i.e., $z_1 = S_{0,1} - \Delta$) is 2.457 m, but the maximum spacing deviation between the last two vehicles (i.e., $z_9 = S_{8,9} - \Delta$) is 0.118 m. Similar observations are made for the vehicle speed and the control input in Fig. 3 respectively.

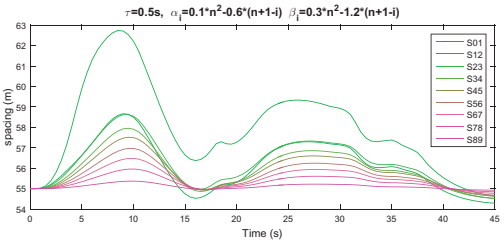

(a) Time history of spacing changes.

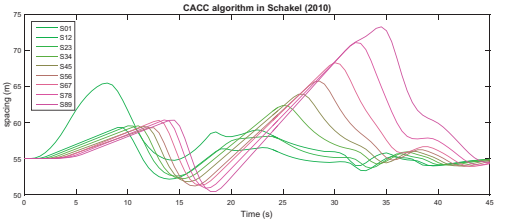

(b) Time history of spacing changes.

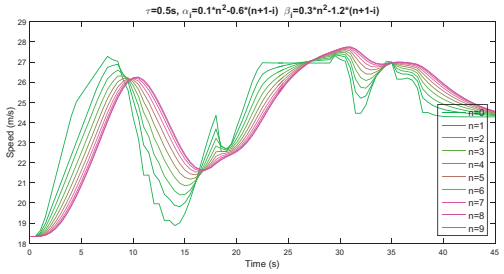

(c) Time history of vehicle speed.

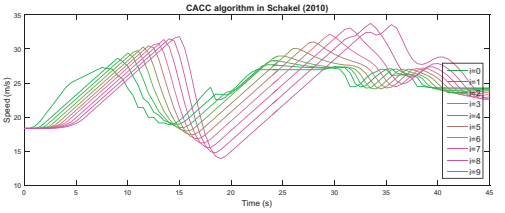

(d) Time history of vehicle speed.

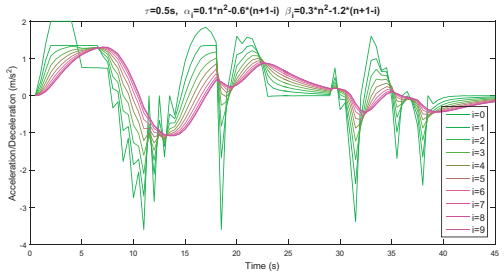

(e) Time history of control input.

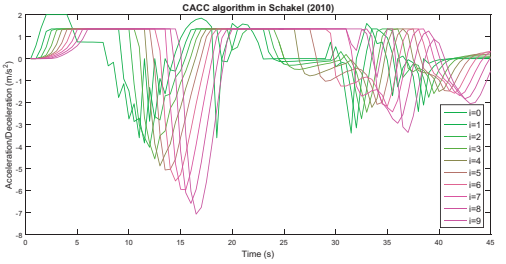

(f) Time history of control input

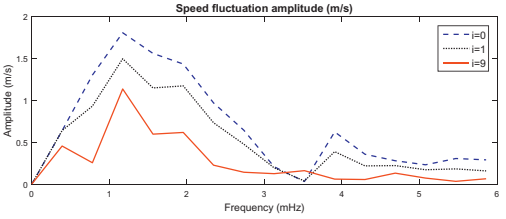

(g) DFT spectrum of detrended speed for $i = 0$, 1 and 9.

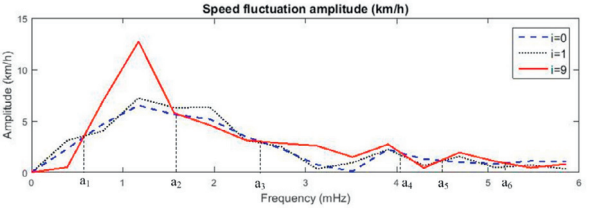

(h) DFT spectrum of detrended speed for $i = 0$, 1 and 9.

Fig. 5. Comparison of the proposed car-following control scheme (left column) and the conventional CACC scheme (right column) in Scenario 3.

- **Scenario 2**. The leading vehicle performs periodic acceleration and deceleration in this scenario. Fig. 4 displays the spacing changes in the platoon. Similar to Scenario 1, the spacing fluctuation becomes smaller as it approaches the platoon tail. For example, the fluctuation amplitude of z_1 is 0.2972 m, that of z_2 decreases to 0.2046 m, and that of z_9 is 0.0134 m. The similar pattern for speed fluctuation can be seen in Fig. 4. Specifically, the speed fluctuation amplitude of the leading vehicle $i = 0$ is 2 m/s. For its following vehicle, the speed fluctuation amplitude decreases to 1.532 m/s. For the last vehicle $i = 9$, that amplitude reduces to 0.3914 m/s. The corresponding control input is shown in Fig. 4. Hence the proposed control scheme effectively dampens the growth of spacing and speed fluctuation in the platoon.
- **Scenario 3**. In this scenario, the leading vehicle moves in a real world traffic flow with significant traffic oscillations. Similar to the last two scenarios, it is shown in Fig. 5(a) that the spacing oscillations are considerably reduced as it is approaching the platoon tail. Even though the leading vehicle is subject to larger and more dramatic acceleration and deceleration than in Scenarios 1 and 2, the spacing $S_{8,9}$ remains almost constant. It is also shown in Fig. 5(c) that the vehicle speed varies smoothly near the platoon tail; the corresponding control input is displayed in Fig. 5(e).

The effect of traffic oscillation of the closed loop system can be evaluated via discrete Fourier transform spectrum (DFT spectrum), which is obtained by the discrete Fourier transform (DFT) for the detrended vehicle speed. The magnitude of DFT spectrum at each frequency shows the magnitude of speed oscillation at that frequency; see Fig. 5(g). The plot shows that the magnitude of speed fluctuation becomes smaller when approaching the platoon tail. For instance, the peak vale for the leading vehicle $i = 0$ is 1.81 m/s, compared with 1.50 m/s for the first following vehicle $i = 1$ and 1.11 m/s for the last following vehicle $i = 9$. Therefore, the proposed control scheme mitigates traffic oscillations substantially.

Our numerical results demonstrate that the proposed control scheme effectively reduces disturbance propagation of relative spacing and speed errors from the leading vehicle to its followers along the platoon. This hints that the proposed control scheme achieves the "string stability" of the platoon (Middleton and Braslavsky, 2010; Seiler et al., 2004; Swaroop, 1997; Swaroop and Hedrick, 1996). Extensions to other information structures will be treated in future.

6.4. Comparison with conventional CACC

In this subsection, we compare the performance of the proposed car-following control scheme and the conventional CACC scheme (Schakel et al., 2010) in Scenario 3. The plots in the left column of Fig. 5 show the results from the proposed car-following control scheme, and the plots in the right column show those from the conventional CACC scheme. In particular, Fig. 5(a) and (b) reveal spacing changes under the two schemes. It is observed that while both the schemes render the vehicles back to the desired spacing eventually, the transient dynamics are dramatically different. For example, the spacing $S_{8,9}$ in Fig. 5(a) is stable and almost constant under the proposed control scheme, whereas the spacing $S_{8,9}$ in Fig. 5(b) demonstrates much larger fluctuation under the CACC scheme. The similar observations can be made by comparing the vehicle speed responses (cf. Fig. 5(c) vs. Fig. 5(d)) and control output responses (cf. Fig. 5(e) vs. Fig. 5(f)). The effects of traffic oscillations are also compared in Fig. 5(g) and (h). It is noted that the magnitude of speed fluctuation under the CACC scheme is increasing significantly when approaching the platoon tail as shown in Fig. 5(h). For example, the peak values of the leading vehicle $i = 0$, the first following vehicle $i = 1$, and the last following vehicle $i = 9$ are 1.81 m/s, 1.97 m/s, and 3.50 m/s, respectively. On the other hand, as shown before, these peak values decrease under the proposed control scheme. It is noticed from our simulation studies that the CACC scheme may smooth traffic oscillation in the platoon at certain frequencies but it does not work well at many others. For example, Fig. 5(h) shows that speed fluctuation is amplified along the platoon at the frequencies in $[a_1, a_2]$, $[a_3, a_4]$ and $[a_5, a_6]$ (i.e. the speed fluctuation at the tail, vehicle $i = 9$ of the platoon is larger than the leading vehicle $i = 0$ and its immediate following vehicle $i = 1$), even though it is dampened at the other frequencies. In contrast, the proposed control scheme dampens speed fluctuation at almost all frequencies. Hence we conclude that the proposed car-following control scheme outperforms the conventional CACC scheme in terms of achieving stable and smoother traffic flows and reducing traffic oscillations.

7. Conclusion

This paper develops a novel platoon car-following control scheme based on constrained optimization and distributed computation by exploiting transportation, control and optimization techniques. Specifically, we consider a platoon of connected and autonomous vehicles, and model it as an interconnected dynamic system subject to acceleration, speed, and safety distance constraints, under the global information structure. A constrained optimization problem is introduced to handle multiple objectives arising from the transient and asymptotic dynamics. Solution properties of this optimization problem are studied and used to develop dual or primal-dual based distributed algorithms. The performance of the proposed control scheme is studied, particularly for the unconstrained linear closed-loop system which is shown to be asymptotically stable. These stability results provide a rule to choose penalty weights in the underlying optimization problem to achieve the desired transient and asymptotic dynamics. Extensive numerical simulations are conducted to illustrate the effectiveness of the proposed distributed algorithms and control scheme in three scenarios. They show that the proposed control scheme effectively reduces the propagation of traffic fluctuation/oscillation along a platoon, which outperforms the conventional cooperative cruise control.

This research is our first attempt toward car-following control of connected and autonomous vehicles. It opens the door to several interesting future research topics summarized below.

(1) Local information structures using communication between neighboring vehicles are suitable for a large sized vehicle platoon. There has been a tremendous interest in car-following control under local information structures and different communication topologies (Desjardins and Chaib-draa, 2011; Li et al., 2015; Lin et al., 2012; Schakel et al., 2010; Wang et al., 2014; Zheng et al., 2016a,b). We will study the impact of local information structures and communication topologies on control performance and distributed computation; the string stability of a platoon will be considered.

(2) The proposed constrained optimization based car-following control is a special case of the general MPC problem (Dunbar and Caveney, 2012; Dunbar and Murray, 2006; Franco et al., 2008; Keviczky et al., 2006; Li et al., 2011; Wang et al., 2014; Zheng et al., 2016a). A future research topic is to extend the current formulation to the general MPC framework by incorporating distributed computation. We also plan to consider general vehicle dynamic models in this extension. Nonlinear closed-loop dynamics under active constraints will be investigated (Hu et al., 2010; Shen and Hu, 2012).

(3) Lastly, we will consider a platoon mixed with human-driven vehicles and connected and autonomous vehicles. Such an extension will make the proposed approach suitable for the near future real world traffic conditions, but it also raises many challenges in dynamics modeling and algorithm design.

Acknowledgments

This research is partially supported by the National Science Foundation awards CMMI-1436786 and CMMI-1554559, and Nayar Prize at Illinois Institute of Technology. The authors are grateful to the two reviewers' constructive comments and instrumental suggestions to relevant research directions in car-following control.

Appendix A

A1. Appendix: Proof of Lemma 3.2

Proof. Let $\mathcal{P}$ denote $\mathcal{P}((x_s, v_s)_{s=0}^n, u_0)$ for the given $(x_s, v_s)_{s=0}^n$ and u_0 in the following proof.

(1) The proofs for the two directions are shown as follows.
(i) $\Rightarrow$ (ii). This is trivial.
(ii) $\Rightarrow$ (i). Note that the following fact follows directly from the argument for Lemma 3.1:
H: For any $\ell = 1, \dots, n-1$, if there exist u_i, $i = 1, \dots, \ell$ such that for each $i = 1, \dots, \ell$, $u_i \in [a_{\min}, a_{\max}]$, $\widetilde{v}_i := v_i + \tau u_i \in [v_{\min}, v_{\max}]$, and $\widetilde{x}_{i-1} - \widetilde{x}_i - [L + r \cdot \widetilde{v}_i - \frac{(\widetilde{v}_i - v_{\min})^2}{2a_{\min}}] \geq 0$, where $\widetilde{x}_i := x_i + \tau v_i + \frac{\tau^2}{2} u_i$, then there exist $u_{\ell+1}, \dots, u_n$ such that $(u_1, \dots, u_n) \in \mathcal{P}$.

Under the assumptions stated in (ii), we first show that $v_i = v_{i-1} = v_{\min}$, $p_i = 0$, and $u_i = u_{i-1} = 0$. For any feasible $u = (u_1, \dots, u_n) \in \mathcal{P}$, recall that $\widetilde{v}_i(u_i) := v_i + \tau u_i \geq v_{\min}$ and $\widetilde{x}_i(u_i) := x_i + \tau v_i + \frac{\tau^2}{2} u_i$. By (16) and the definitions of p_i in (14) and q_i in (15), we have

$$\begin{aligned} &\widetilde{x}_{i-1}(u_{i-1}) - \widetilde{x}_i(u_i) - \left[L + r\widetilde{v}_i(u_i) - \frac{(\widetilde{v}_i(u_i) - v_{\min})^2}{2a_{\min}} \right] \\ &= p_i + \tau \left\{ v_{i-1} + \frac{\tau u_{i-1}}{2} - q_i(u_i) \right\} \geq p_i + \tau \left[v_{\min} - q_i(u_i) \right]. \end{aligned}$$

Note that if $v_{\min} < v_i \leq v_{\max}$, then by the claim shown in the proof of Lemma 3.1, there exists $\widehat{u}_i$ with $a_{\min} < \widehat{u}_i < a_{\max}$ such that $v_{\min} < \widetilde{v}_i(\widehat{u}_i) < v_{\max}$, and $q_i(\widehat{u}_i) < v_{\min}$. The latter implies that $\widetilde{x}_{i-1}(u_{i-1}) - \widetilde{x}_i(u_i) - [L + r\widetilde{v}_i(u_i) - \frac{(\widetilde{v}_i(u_i) - v_{\min})^2}{2a_{\min}}] > 0$. This shows via Fact **H** that for any feasible $u = (u_1, \dots, u_n) \in \mathcal{P}$ and any small $\varepsilon > 0$, there exist $u'_{i+1}, \dots, u'_n$ (depending on ε) such that $(u_1, \dots, u_{i-1}, \widehat{u}_i + \varepsilon, u'_{i+1}, \dots, u'_n) \in \mathcal{P}$. This contradicts the assumption that u_i is singleton stated in (ii). Hence we must have $v_i = v_{\min}$. Besides, we further claim $p_i = 0$. Suppose not, i.e., $p_i > 0$. Since $q_i(0) = v_i = v_{\min}$, we see that if $\widehat{u}_i$ is any sufficiently small positive number, then $a_{\min} < \widehat{u}_i < a_{\max}$, $v_{\min} < \widetilde{v}_i(\widehat{u}_i) < v_{\max}$, and $p_i + \tau[v_{\min} - q_i(\widehat{u}_i)] > 0$ by the continuity of q_i. By the similar argument as before, we obtain multiple feasible u_i's, contradicting (ii). This shows that $p_i = 0$. Thus by (16), $v_i = v_{\min}$, and q_i defined in (15), we have, for any feasible $u = (u_1, \dots, u_i) \in \mathcal{P}$,

$$\widetilde{x}_{i-1}(u_{i-1}) - \widetilde{x}_i(u_i) - \left[L + r\widetilde{v}_i(u_i) - \frac{(\widetilde{v}_i(u_i) - v_{\min})^2}{2a_{\min}} \right] = \tau \left[v_{i-1} + \frac{\tau u_{i-1}}{2} - q_i(u_i) \right].$$

If $v_{i-1} > v_{\min}$, it follows from $\widetilde{v}_{i-1}(u_{i-1}) \geq v_{\min}$ that $v_{i-1} + \frac{\tau u_{i-1}}{2} = \frac{v_{i-1} + \widetilde{v}_{i-1}(u_{i-1})}{2} > v_{\min}$. Hence by $q_i(0) = v_{\min}$ and the continuity of $q_i(\cdot)$, we have $v_{i-1} + \frac{\tau u_{i-1}}{2} - q_i(u_i) > 0$ for any sufficiently small positive u_i. Similarly, if $u_{i-1} > 0$, in view of $v_{i-1} \geq v_{\min}$, we have $v_{i-1} + \frac{\tau u_{i-1}}{2} - q_i(u_i) > 0$ for any sufficiently small positive u_i. This shows that in both cases, any sufficiently small positive u_i is feasible, a contradiction to (ii). Hence we must have $v_{i-1} = v_{\min}$ and $u_{i-1} \leq 0$. In light of (15),

$$\begin{aligned} &\widetilde{x}_{i-1}(u_{i-1}) - \widetilde{x}_i(u_i) - \left[L + r\widetilde{v}_i(u_i) - \frac{(\widetilde{v}_i(u_i) - v_{\min})^2}{2a_{\min}} \right] \\ &= \tau \left[v_{\min} + \frac{\tau u_{i-1}}{2} - q_i(u_i) \right] = \frac{\tau^2 u_{i-1}}{2} - \tau \left(\frac{\tau}{2} + r \right) u_i + \frac{\tau^2 u_i^2}{2a_{\min}} \geq 0. \end{aligned} \tag{31}$$

Since $\widetilde{v}_i(u_i) = v_{\min} + \tau u_i \geq v_{\min}$, we have $u_i \geq 0$. Further, noting that $u_{i-1} \leq 0$, $r + \frac{\tau}{2} > 0$ and $a_{\min} < 0$, we must have $u_i = 0$ and $u_{i-1} = 0$.
For the given i, it has been shown above that $u_{i-1} = 0$ for any $u = (u_1, \dots, u_n) \in \mathcal{P}$. Hence we deduce via the same argument as before that $p_{i-1} = 0$, $v_{i-1} = v_{i-2} = v_{\min}$, and $u_{i-2} = 0$ for any $u \in \mathcal{P}$. Continuing this process and by induction, we have $p_1 = \cdots = p_i = 0$, $v_0 = v_1 = \cdots = v_i = v_{\min}$, and $u_0 = u_1 = \cdots = u_i = 0$ for any $u = (u_1, \dots, u_n) \in \mathcal{P}$. This yields ($i$).

(2) Let $u_0 = 0$ and $\ell \in \{1, \dots, n\}$ be the largest index such that $p_1 = \cdots = p_\ell = 0$ and $v_0 = v_1 = \cdots = v_\ell = v_{\min}$. It follows from the proof of statement (1), particularly the argument around (31), that $u_1 = 0$ for any $u = (u_1, \dots, u_n) \in \mathcal{P}$. By induction, we further have $u_2 = \cdots = u_\ell = 0$ for any $u = (u_1, \dots, u_n) \in \mathcal{P}$.
Consider $i = \ell + 1$, for which either $p_i > 0$ or $v_i > v_{\min}$. Fix $u := (0, \dots, 0, u_{\ell+1}, u_{\ell+2}, \dots u_n) \in \mathcal{P}$. In light of statement (1), there exists $u'_{\ell+1} \neq u_{\ell+1}$ such that $(0, \dots, 0, u'_{\ell+1}, u_{\ell+2}, \dots u_n) \in \mathcal{P}$. Since $\mathcal{P}$ is a convex set, $(0, \dots, 0, \widetilde{u}_{\ell+1}, u_{\ell+2}, \dots u_n) \in \mathcal{P}$ for any $\widetilde{u}_{\ell+1} \in \mathcal{I}_{\ell+1}$, where $\mathcal{I}_{\ell+1}$ is the line segment in $\mathbb{R}$ joining $u_{\ell+1}$ and $u'_{\ell+1}$.
When $i = \ell + 2$, we have either (i) $[v_i > v_{\min}]$ or (ii) $[v_i = v_{\min}$ and $p_i > 0]$. For case (i), it follows from the proof for Lemma 3.1 that there is a compact interval $\mathcal{I}_{\ell+2}$ such that any $\widetilde{u}_{\ell+2} \in \mathcal{I}_{\ell+2}$ satisfies: $a_{\min} < \widetilde{u}_{\ell+2} < a_{\max}$, $v_{\min} < \widetilde{v}_{\ell+2}(u_{\ell+2}) := v_{\ell+2} + \tau \widetilde{u}_{\ell+2} < v_{\max}$, and $q_{\ell+2}(\widetilde{u}_{\ell+2}) < v_{\min}$, which, by (16), implies that $-g(\widetilde{u}_{\ell+1}, \widetilde{u}_{\ell+2}) = \widetilde{x}_{\ell+1}(\widetilde{u}_{\ell+1}) - \widetilde{x}_{\ell+2}(\widetilde{u}_{\ell+2}) - [L + r\widetilde{v}_{\ell+2}(\widetilde{u}_{\ell+2}) - \frac{(\widetilde{v}_{\ell+2}(\widetilde{u}_{\ell+2}) - v_{\min})^2}{2a_{\min}}] > 0$ for any $\widetilde{u}_{\ell+1} \in \mathcal{I}_{\ell+1}$. For case (ii), the proof for Lemma 3.1 and (16) also show that there is an interval $\mathcal{I}_{\ell+2} := [0, \widetilde{\varepsilon}]$ for a sufficiently small $\widetilde{\varepsilon} > 0$ such that each $\widetilde{u}_{\ell+2} \in \mathcal{I}_{\ell+2}$ satisfies the above inequalities for any $\widetilde{u}_{\ell+1} \in \mathcal{I}_{\ell+1}$.
Repeating the above argument for $i = \ell + 3, \dots, n$, we obtain compact intervals $\mathcal{I}_j$ with $j = \ell + 1, \dots, n$ such that for any $\widetilde{u}_j \in \mathcal{I}_j$, $(0, \dots, 0, \widetilde{u}_{\ell+1}, \dots \widetilde{u}_n) \in \mathcal{P}$. Let $\widehat{u}_j$ be the middle point of each $\mathcal{I}_j$, and $\varepsilon > 0$ be sufficiently small. It is easy to verify that statement (2) holds. □

A2. Appendix: primal-dual and extra-gradient based distributed algorithm

Motivated by the primal-dual based distributed algorithm in Koshal et al. (2009, 2011) and the extra-gradient method for pseudo monotone variational inequalities (Facchinei and Pang, 2003, Section 12.1.2), we consider the following algorithm:

$$u_i^{m+\frac{1}{2}} = \Pi_{\mathcal{X}_i}\big(u_i^m - \xi\, \nabla_{u_i}\mathcal{L}(u^m, \lambda^m)\big), \quad \lambda_i^{m+\frac{1}{2}} = \Pi_{\mathcal{I}_i}\big(\lambda_i^m + \xi\, g_i(u^m)\big), \quad \forall\, i = 1, \dots, n,$$

$$u_i^{m+1} = \Pi_{\mathcal{X}_i}\big(u_i^m - \xi\, \nabla_{u_i}\mathcal{L}(u^{m+\frac{1}{2}}, \lambda^{m+\frac{1}{2}})\big), \quad \lambda_i^{m+1} = \Pi_{\mathcal{I}_i}\big(\lambda_i^{m+\frac{1}{2}} + \xi\, g_i(u^{m+\frac{1}{2}})\big), \quad \forall\, i = 1, \dots, n,$$

where $\xi > 0$ is the step-length.

To find a suitable ξ for numerical convergence, we introduce the following function:

$$F(u, \lambda) := \begin{bmatrix} \nabla_u \mathcal{L}(u, \lambda) \\ -\nabla_\lambda \mathcal{L}(u, \lambda) \end{bmatrix} = \begin{bmatrix} \nabla J(u) + \sum_{i=1}^n \lambda_i \nabla g_i(u) \\ -g(u) \end{bmatrix}.$$

Recall that each g_i is a convex quadratic function given by $g_i(u) := \frac{1}{2}u^T E_i u + h_i^T u + \varphi_i$, where E_i is given in (11). Let $\omega := \max_{u \in \mathcal{X}} \|u\|_2$. Define the following positive constants:

$$M_g := \sqrt{\sum_{i=1}^n \big(\omega \|E_i\|_2 + \|h_i\|_2\big)^2}, \qquad \bar{L} := \sqrt{\Big(\mu_{\max}(H + \sum_{i=1}^n \eta_i E_i) + M_g\Big)^2 + (M_g)^2}, \tag{32}$$

where $\eta_i \geq 0$ is defined in (21).

Lemma A.1. *The function F is monotone on $\mathcal{X} \times \mathbb{R}^n_+$ and is Lipschitz continuous on $\mathcal{X} \times \mathcal{D}'$ with the Lipschitz constant $\bar{L}$.*

Proof. The monotonicity follows from the similar argument for (Koshal et al., 2011, Lemma 3.4). In fact, by this argument, it can be shown that for any $(u, \lambda), (u', \lambda') \in \mathcal{X} \times \mathbb{R}^n_+$, $\big(F(u, \lambda) - F(u', \lambda')\big)^T (u - u', \lambda - \lambda') \geq \mu_{\min}(H) \cdot \|u - u'\|_2^2 \geq 0$. To establish the Lipschitz constant $\bar{L}$, we deduce from

$$\nabla_{(u,\lambda)} F(u, \lambda) = \begin{bmatrix} H + \sum_{i=1}^n \lambda_i E_i & (E_1 u + h_1), \cdots\cdots, (E_n u + h_n) \\ -(E_1 u + h_1), \cdots\cdots, -(E_n u + h_n) & 0 \end{bmatrix}$$

that $\nabla_{(u,\lambda)} F(u, \lambda)$ is a positive semidefinite (but not symmetric) matrix. By the similar argument for (Koshal et al., 2011, Lemma 3.4), we have $\|\nabla_{(u,\lambda)} F(u, \lambda)\|_2 \leq \bar{L}$ for any $(u, \lambda) \in \mathcal{X} \times \mathcal{D}'$. In light of the mean-value inequality, $\bar{L}$ is the desired Lipschitz constant. □

Since the function F is monotone on $\mathcal{X} \times \mathcal{D}'$, it is pseudo monotone on $\mathcal{X} \times \mathcal{D}'$. By (Facchinei and Pang, 2003, Theorem 12.1.11) and (Facchinei and Pang, 2003, Theorem 12.6.4), we obtain the following numerical convergence result.

Proposition A.1. *Let the step-length ξ be $0 < \xi < 1/\bar{L}$. Then the sequence $((u^m, \lambda^m))$ generated by the primal-dual algorithm converges to an optimal solution (u_*, λ_*) at least R-linearly.*

References

Cook, P.A., 2007. Stable control of vehicle convoys for safety and comfort. IEEE Trans. Autom. Control 52 (3), 526–531.

Desjardins, C., Chaib-draa, B., 2011. Cooperative adaptive cruise control: a reinforcement learning approach. IEEE Trans. Intell. Transp. Syst. 12 (4), 1248–1260.

Dunbar, W.B., Caveney, D.S., 2012. Distributed receding horizon control of vehicle platoons: stability and string stability. IEEE Trans. Autom. Control 57 (3), 620–633.

Dunbar, W.B., Murray, R.M., 2006. Distributed receding horizon control for multi-vehicle formation stabilization. Automatica 42 (4), 549–558.

Facchinei, F., Pang, J.S., 2003. Finite-Dimensional Variational Inequalities and Complementarity Problems. Springer-Verlag, New York.
Franco, E., Magni, L., Parisini, T., Polycarpou, M.M., Raimondo, D.M., 2008. Cooperative constrained control of distributed agents with nonlinear dynamics and delayed information exchange: A stabilizing receding-horizon approach. IEEE Trans. Autom. Control 53 (1), 324–338.
Hao, H., Barooah, P., 2013. Stability and robustness of large platoons of vehicles with double-integrator models and nearest neighbor interaction. Int. J. Robust Nonlinear Control 23 (18), 2097–2122.
Hu, J., Shen, J., Zhang, W., 2010. Generating functions of switched linear systems: analysis, computation, and stability applications. IEEE Trans. Autom. Control 56 (5), 1059–1074.
Jin, I., Orosz, G., 2014. Dynamics of connected vehicle systems with delayed acceleration feedback. Transp. Res. Part C 46, 46–64.
Jovanović, M.R., Bamieh, B., 2005. On the ill-posedness of certain vehicular platoon control problems. IEEE Trans. Autom. Control 50 (9), 1307–1321.
Keviczky, T., Borrelli, F., Balas, G.J., 2006. Decentralized receding horizon control for large scale dynamically decoupled systems. Automatica 42 (12), 2105–2115.
Koshal, J., Nedić, A., Shanbhag, U.V., 2009. Distributed multiuser optimization: algorithms and error analysis. In: Proc. IEEE Conf. Decision and Control, pp. 4372–4377. Shanghai
Koshal, J., Nedic, A., Shanbhag, U.V., 2011. Multiuser optimization: distributed algorithms and error analysis. SIAM J. Optim. 21 (3), 1046–1081.
Laval, J.A., Leclercq, L., 2010. A mechanism to describe the formation and propagation of stop-and-go waves in congested freeway traffic. Philos. Trans. R. Soc. London A 368 (1928), 4519–4541.
Li, S., Li, K., Rajamani, R., Wang, J., 2011. Model predictive multi-objective vehicular adaptive cruise control. IEEE Trans. Control Syst. Technol. 19 (3), 556–566.
Li, S.E., Zheng, Y., Li, K., Wang, J., 2015. An overview of vehicular platoon control under the four-component framework. In: IEEE Intelligent Vehicles Symposium. IEEE, pp. 286–291.
Lin, F., Fardad, M., Jovanović, M.R., 2012. Optimal control of vehicular formations with nearest neighbor interactions. IEEE Trans. Autom. Control 57 (9), 2203–2218.
May, A.D., 1989. Traffic Flow Fundamentals. Prentice Hall.
Middleton, R.H., Braslavsky, J.H., 2010. String instability in classes of linear time invariant formation control with limited communication range. IEEE Trans. Autom. Control 55 (7), 1519–1530.
Monteil, J., Billot, R., Sau, J., Faouzi, E., 2014. Linear and weakly nonlinear stability analyses of cooperative car-following models. IEEE Trans. Intell. Transp. Syst. 15 (5), 2001–2003.
Nakayama, A., Sugiyama, Y., Hasebe, K., 2002. Effect of looking at the car that follows in an optimal velocity model of traffic flow. Phys. Rev. E 65, 1–6.
Naus, G., Vugts, R., Ploeg, J., van de Molengraft, M., Steinbuch, M., 2010. String-stable CACC design and experimental validation: a frequency-domain approach. IEEE Trans. Veh. Technol. 59 (9), 4268–4279.
Naus, G., Vugts, R., Ploeg, J., van de Molengraft, R., Steinbuch, M., 2010. Cooperative adaptive cruise control, design and experiments. In: In American Control Conference, pp. 6145–6150.
Oncu, S., Ploeg, J., van de Wouw, N., Nijmeijer, H., 2014. Cooperative adaptive cruise control: network-aware analysis of string stability. IEEE Trans. Intell. Transp. Syst. 15 (4), 1527–1537.
Polyak, B.T., 1987. Introduction to Optimization. Optimization Software, Inc., New York.
Qin, W., Gomez, M., Orosz, G., 2014. Stability analysis of connected cruise control with stochastic delays. In: In American Control Conference, pp. 4624–4629.
Rajamani, R., Shladover, S.E., 2001. An experimental comparative study of autonomous and co-operative vehicle-follower control systems. Transp. Res. Part C 9(1), 15–31.
Richards, A., How, J., 2004. A decentralized algorithm for robust constrained model predictive control. In: Proceedings of the American Control Conference, vol. 5, pp. 4261–4266.
Seiler, P., Pant, A., Hedrick, K., 2004. Disturbance propagation in vehicle strings. IEEE Trans. Autom. Control 49 (10), 1835–1842.
Shen, J., Hu, J., 2012. Stability of discrete-time switched homogeneous systems on cones and conewise homogeneous inclusions. SIAM J. Control Optim. 50 (4), 2216–2253.
Shladover, S., VanderWerf, J., Miller, M. A., Kourjanskaia, N., Krishnan, H., 2001. Development and performance evaluation of avcss deployment sequences to advance from today's driving environment to full automation. California Partners for Advanced Transit and Highways (PATH).
Swaroop, D., 1997. String stability of interconnected systems: An application to platooning in automated highway systems. California Partners for Advanced Transit and Highways (PATH).
Swaroop, D., Hedrick, J.K., 1996. String stability of interconnected systems. IEEE Trans. Autom. Control 41 (3), 349–357.
Swaroop, D., Hedrick, J.K., 1999. Constant spacing strategies for platooning in automated highway systems. J. Dyn. Syst. Meas. Control 121 (3), 462–470.
Schakel, W.W.J., Arem, B.V., Netten, B.D., 2010. Effects of cooperative adaptive cruise control on traffic flow stability. In: 13th International IEEE Conference on Intelligent Transportation Systems (ITSC), pp. 759–764.
van Arem, B., Driel, C.J.V., Visser, R., 2006. The impact of cooperative adaptive cruise control on traffic-flow characteristics. IEEE Trans. Intell. Transp. Syst. 7 (4), 429–436.
van Arem, B., Driever, H., Feenstra, P., Ploeg, J., Klunder, G., Wilmink, I., Netten, B., 2007. Design and evaluation of an integrated full-range speed assistant. Summary of research, TNO Traffic and Transport.
Wang, M., Daamen, W., Hoogendoorn, S.P., van Arem, B., 2014. Rolling horizon control framework for driver assistance systems. part ii: Cooperative sensing and cooperative control. Transp. Res. Part C 40, 290–311.
Zheng, Y., Li, S.E., Li, K., Borrelli, F., Hedrick, J.K., 2016. Distributed model predictive control for heterogeneous vehicle platoons under unidirectional topologies. IEEE Transactions on Control Systems Technology, accepted.
Zheng, Y., Li, S.E., Wang, J., Cao, D., Li, K., 2016. Stability and scalability of homogeneous vehicular platoon: Study on the influence of information flow topologies. IEEE Trans. Intell. Transp. Syst. 17 (1), 14–26.